RELATIONSHIPS BETWEEN CRYSTAL STRUCTURE, BONDING AND THERMAL STABILITY OF AMPHIBOLES

by

KWO-LING CHYI

Dissertation submitted to the faculty of the

Virginia Polytechnic Institute and State University

in partial fulfillment of the requirements for the degree of

Doctor of Philosophy

in

Geological Sciences

APPROVED:

G. V. Gibbs, Co-chairman	D. A. Hewitt, Co-chairman
F. D. Bloss	M. C. Gilbert
J. D. Rimstidt	

June, 1987
Blacksburg, Virginia

Relationships between crystal structure, bonding and thermal stability of amphiboles

by

Kwo-Ling Chyi

Gerald V. Gibbs, Co-Chairman

David A. Hewitt, Co-Chairman

Dept. of Geological Sciences

(ABSTRACT)

The complexities in structure and chemical composition of the amphiboles and the wide range of their occurrence suggest that the amphiboles are potential index minerals for the physical conditions of their formation. Hydrothermal stability studies of several amphibole end-members have demonstrated that the $FeMg_{-1}$ substitution produces a wide spread in thermal stability. The crystal structure, upon substitution, responds to the differences in cation size and site occupancy, but the changes are small.

In order to correlate the observed stability variation with the observed differences in crystal structure of amphiboles, structure parameters as well as calculated bond strengths, Madelung site energies, and average bond overlap populations obtained from Extended Hückel Molecular Orbital (EHMO) calculation for different cation sites, were examined. Among the examined structural parameters, calculated Madelung site potentials, and bond strength, only the parameters involving bonds between the M(1)- and M(3)-cations with OH show higher correlations with the thermal stability as compared to those of the M(2)- and M(4)-cations. This reflects the dehydration nature of the amphibole break-down reaction, since the OH bonding with seems important in controling the thermal stability.

Infrared absorption spectra of amphiboles show the fine structure of the hydroxyl group. The frequency of the absorption band is related directly to the strength of the OH bond. Positive correlations exist between thermal stability and OH-stretching frequency for different amphibole end-members at different temperatures. For epidote minerals, as well as for muscovite and phlogopite, high OH-stretching frequencies also correlated with the minerals having higher thermal stability. These correlations indicate that the thermal stability of many hydrous minerals may be significantly related the localized force field around the OH bond.

The crystal structure of grunerite Klein No. 9A has been refined and compared with grunerite Klein No. 1 (Finger, 1969) and cummingtonite (Ghose, 1961; Fisher, 1966). The results show that the substitution of Fe for Mg into the cummingtonite-grunerite structure not only enlarges the octahedral layer but also affects the size of the T(1) and T(2) tetrahedra and thus increases strain on the octahedral and tetrahedral linkage. The high thermal expansion of the octahedral layer and the negligible effect of heating on the tetrahedral layer substantially increase the strain on the structure. This may also explain why the Fe-rich end member decomposes at a lower temperature than its Mg-analogue, the structure of which can accommodate the build up of strain with increasing temperature.

ACKNOWLEDGEMENTS

I would like to express my deepest appreciation to Professors Gerald V. Gibbs and David A. Hewitt for their assistance and financial support. Acknowledgements are also extended to Drs. F. Donald Bloss, Richard V. Dietrich, M. Charles Gilbert and J. Donald Rimstidt for their critical reading of the manuscript. Special thanks are due to Ms. Mary Mrose for giving me the opportunity to receive two years scholarship from the American Federation of Mineralogical Socities. Drs. W.G. Ernst, R.W. Charles, and C. Klein are thanked for providing the samples for this study. I also appreciate the technical assistance I received from Don Bodell, Jim Light, Todd Solberg and Sharon Chiang. I thank Dr. Lucian Zelazny, Agronomy Department for granting me the access to his laboratory for the IR sample preparations and IR spectra collection. Mr. Bin Lee, Chemistry Department is thanked for his help in gaining the access to a Nicolet MX-1 FTIR unit. V.P.I. and S.U. is thanked for offering me four-years' financial support as a teaching assistant. I would also like to thank my family members for their support and considerations.

To my deepest regret, I could not deliver my appreciations to the late Professor David R. Wones and my deceased father. Without Professor Wones's guidance and support, I would not have accomplished this study. Without my father's inspiriation, I would never have pursued my graduate studies. They are keenly missed.

TABLE OF CONTENTS

LIST OF FIGURES

LIST OF TABLES

CHAPTER 1. INTRODUCTION

The amphiboles, an important group of rock forming minerals, occur in a wide variety of igneous and metamorphic rocks. There are both monoclinic and orthrohombic amphiboles. Most of the amphibole end-members that have been studied hydrothermally are monoclinic with space group C2/m (Boyd, 1959; Ernst, 1960; 1962; 1966; Charles, 1975; Forbes, 1977; Semet, 1973; Thomas, 1982). The C2/m amphibole structure has two nonequivalent tetrahedral sites, T(1) and T(2), three nonequivalent octahedral sites, M(1), M(2) and M(3), one M(4) site surrounded by eight anions, and one A site surrounded by twelve anions. The T(1) site is coordinated by three bridging oxygens, O(5), O(6) and O(7); and one nonbridging oxygen O(1); the T(2) site is coordinated by two bridging oxygens, O(5) and O(6), and two nonbridging oxygens, O(2) and O(4). The double chain structure is linked by bridging oxygens O(5) and O(6) lengthwise and by O(7) crossing the chain. Along the chain, T(1) and T(2) tetrahedra shared corners, and across the chain T(1) tetrahedra share corners (Ernst, 1968). The relative positions of the different cation sites are shown in Figure 1.1.

The orthorhombic Fe-Mg amphibole with space group Pnma (Figure 1.2) has also been investigated (Chernosky and Autio, 1979; Cameron, 1975; Popp *et al.*, 1976). The difference between Pnma structure type and C2/m structure type is the absence of a 2-fold axis in the Pnma structure. This results in two different tetrahedral chains, A and B, and the different stacking sequence (Figure 1.3) leads to the doubling of the *a* cell edge. Other than the tetrahedral sites, both the Pnma and the C2/m structures have the same cation sites. Table 1.1 gives the basic site symmetries and occupancies in these two

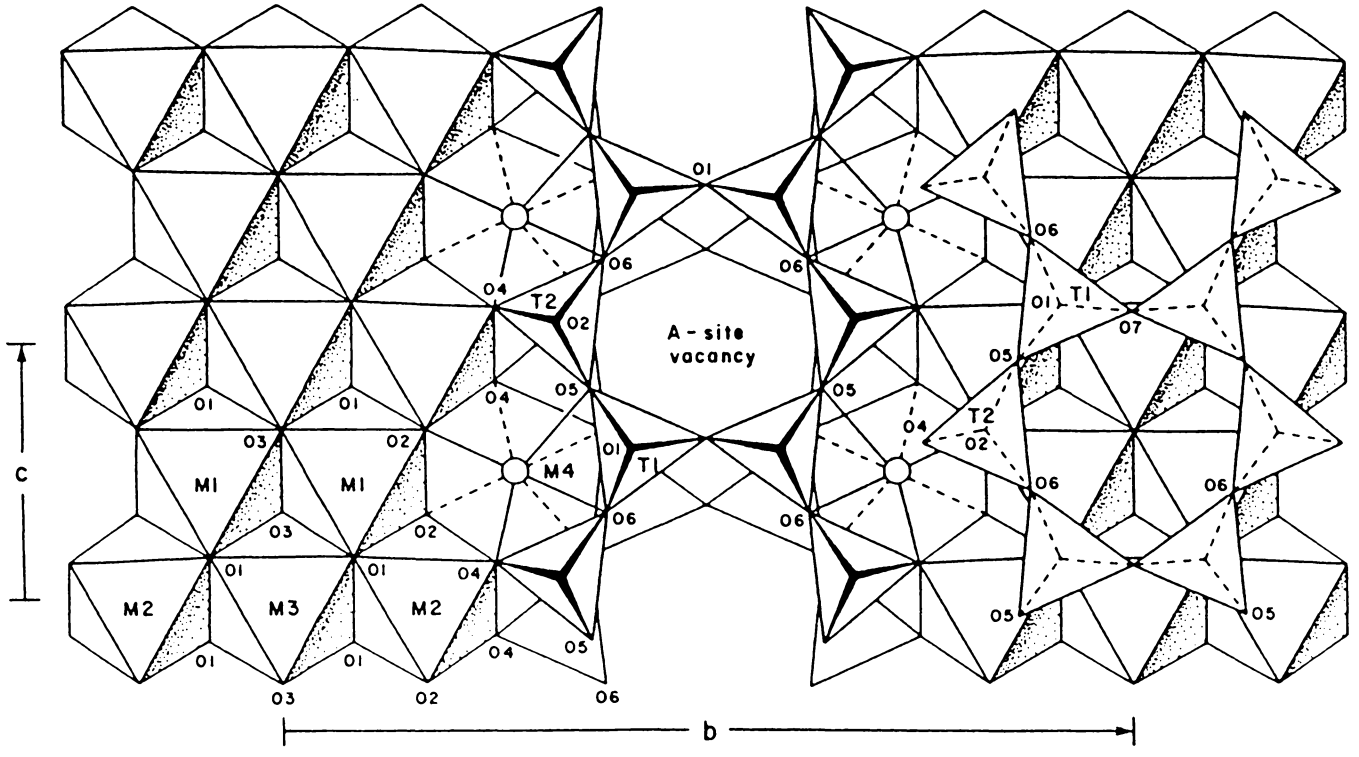

Figure 1.1 The C2/m amphibole structure projected on to (100)
(after Cameron and Papike, 1979).

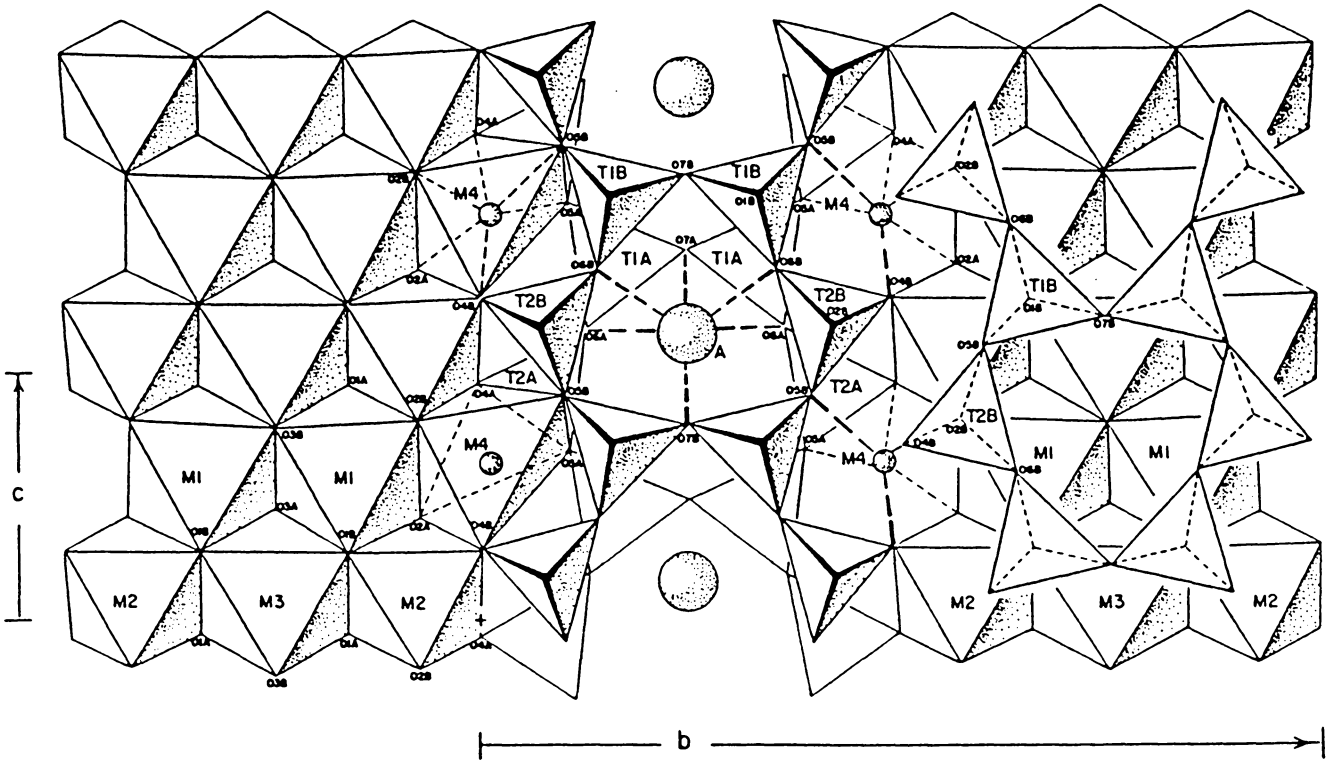

Figure 1.2 The Pnma amphibole structure projected on to (100)
(after Cameron and Papike, 1979).

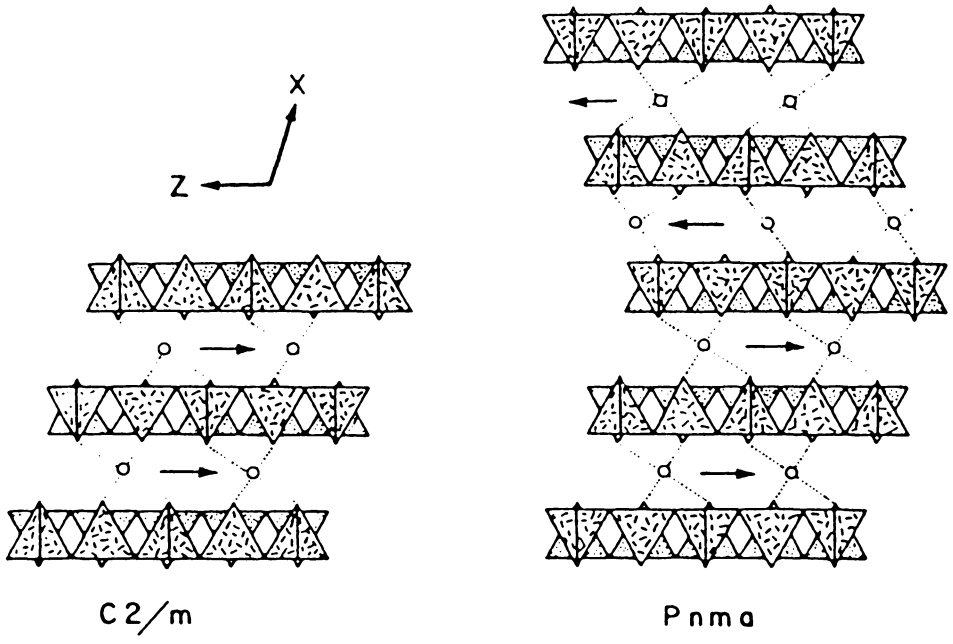

Figure 1.3 Schematic representation of the stacking sequences of layers as projected down Y for the C2/m and Pnma structure-types (after Gibbs, 1966).

Table 1.1 Site chemistry and symmetry for C2/m and Pnma amphiboles

C2/m			Pnma			
Site	**Sym**	**C.N.**	**Site**	**Sym**	**C.N.**	**Site Chemistry**
A	2/m	12	A	m	12	Na, K
M(1)	2	6	M(1)	1	6	Mg, Fe^{+2} Fe^{+3}, Al (Mn, Ti, Li)
M(2)	2	6	M(2)	1	6	Mg, Fe^{+2}, Fe^{+3}, Al (Mn, Ti, Li)
M(3)	2/m	6	M(3)	m	6	Mg, Fe^{+2}, Fe^{+3}, Al (Mn, Ti, Li)
M(4)	2	8	M(4)	1	8	Na, Ca, Fe^{+2}, Mg (Li, Mn)
T(1)	1	4	T(1A)	1	4	Si, Al
			T(1B)	1	4	Si, Al
T(2)	1	4	T(2A)	1	4	Si, Al
			T(2B)	1	4	Si, Al

Elements in parentheses also occur in natural samples.

amphibole systems. Elements in parentheses also occur in natural amphiboles.

The chemistry of the amphibole group is extremely complex because of the extensive substitutions that take place in the cation sites. The type and extent of substitution is determined by the chemical environment and PT conditions of formation, by the size of the site and of the available cation, and by the requirement for electrostatic neutrality in the structure.

In the last three decades, considerable efforts have been expended to determine the stability fields of different amphibole end-members (Boyd, 1959; Ernst, 1960, 1962, 1966; Greenwood, 1963; Gilbert, 1966; Troll and Gilbert, 1972; Gilbert and Briggs, 1974; Charles, 1975, 1977; Thomas, 1977, 1982; Forbes, 1977; Chernosky and Autio, 1979; Semet and Ernst, 1981). These studies have increased understanding of the phase relations between amphiboles and coexisting minerals and have helped in interpreting the parageneses of amphibole-bearing rocks.

Hydrothermal experiments show that under the same pressures and same buffer conditions the Fe^{2+} end-members decompose at temperatures about 300 to 400°C lower than their Mg-analogues (Table 1.2). In each of the pairs, similar phases are commonly involved in their decomposition reactions and the main difference is the Fe- or Mg-occupancy of the octahedral sites M(1), M(2), and M(3). Wones (1981) pointed out that the inherent difference in bond strength between Fe and Mg when bonded to OH leads to the difference in thermal stability. The cell parameters show only slight differences as a result of this substitution.

The O(3) site is occupied by different elements including OH^-, O^{2-}, F^-, and Cl^- (Deer *et al.*, 1963). Thus, the stability relations of amphiboles depend

Table 1.2 Decomposition temperatures of synthetic amphiboles at different pressures

Synthetic Mineral	Temperature (°C) at 500 (bars)	1000 (bars)	2000 (bars)	Reference
Ferrotremolite $Ca_2Fe_5Si_8O_{22}(OH)_2$	424	452	489	Ernst, 1966
Tremolite $Ca_2Mg_5Si_8O_{22}(OH)_2$	775	836	870	Boyd, 1959
Ferropargasite $NaCa_2Fe_4AlSi_6Al_2O_{22}(OH)_2$	550	605	636	Gilbert, 1966
Pargasite $NaCa_2Mg_4AlSi_6Al_2O_{22}(OH)_2$	950	1010	-	Boyd, 1959
Ferrorichterite $NaCaNaFe_5Si_8O_{22}(OH)_2$	526	535	539	Charles, 1975
Richterite $NaCaNaMg_5Si_8O_{22}(OH)_2$	1015	1028	-	Charles, 1975
Hastingsite $NaCa_2Fe_4FeSi_6Al_2O_{22}(OH)_2$	530	616	665	Thomas, 1977
Magnesiohastingsite $NaCa_2Mg_4FeSi_6Al_2O_{22}(OH)_2$	930	1010	-	Semet & Ernst, 1981

not only on total pressure and temperature but also on the fugacities of O_2, H_2O, F, and Cl. The replacement of OH^- by F^- significantly raises the thermal stability of an amphibole (Comeforo and Kohn, 1954; Ernst, 1962; Gilbert and Troll, 1974). However, Cameron and Gibbs (1973) found no significant differences in the structures of tremolite and fluor-tremolite to correlate with the higher thermal stability of fluor-tremolite, and concluded that the stronger Mg-F bond, as compared to the Mg-OH bond, leads to the stabilization of fluor-tremolite at higher temperature. There are no other reported studies correlating the structure or bonding of amphiboles to their thermal stability limits. High temperature crystal structure studies of selected amphiboles (Sueno *et al.*, 1972, 1973; Cameron *et al.*, 1973a, b) show that the octahedra expand rapidly but the tetrahedra are virtually unaffected with increasing temperature. Hence, increasing temperature might affect the structure in the same way as substituting large cations into the structure. However, no systematic correlation between structure, bonding and thermal stability of amphiboles has been recorded.

Modest differences in composition and structure cause significant changes in the energetics of the phases and, therefore, large differences in thermal stability. The purpose of this study is to establish qualitative correlations between the crystal structure, bonding properties, and thermal stability of amphiboles.

It is necessary to have both thermal expansion and compressibility data for each structure in order to compare structures at any pressures and temperatures different from 1 atmosphere and 25°C. Amphibole decomposition reactions are fundamentally dehydration reactions. Using the data of Burnham *et al.* (1969) for the properties of water and taking all of these

reactions to be equilibria involving only pure solids and pure water, the stability curves are plotted as a function of $\log f H_2O$ and 1/T (K) at 1 atm in Figure 1.4. The stability field of each amphibole is to the right side of its corresponding line. As can be seen, at a constant temperature, the more stable phases are associated with lower minimum $\log f H_2O$ values.

Hazen and Prewitt (1977) found that the thermal expansion coefficient of divalent cation-oxygen bonds is constant when the cations have the same coordination number. High temperature crystal structure analyses (Sueno *et al.*, 1972, 1973; Cameron *et al.*, 1973a, b) demonstrate similar thermal expansion on octahedral bonds but negligible apparent thermal expansion on tetrahedral bonds. These indicate that structural parameters, without adjustment for temperature differences, can be compared with thermal stability data at different temperatures and exhibit the same trend.

Crystal structure analyses most nearly representative of chemical end-members were selected from published studies in order to compare bonding properties with the thermal stability data of certain synthetic amphibole end-members. However, as is reflected by differences in cell parameters (Table 1.3), they do differ from the synthetic end-members in composition and perhaps in structure as well. Their structural parameters as well as their calculated bond strengths, Madelung site energies, and average bond overlap populations obtained from Extended Hückel Molecular Orbital (EHMO) calculation for different cation sites, were used to establish correlations between structure and thermal stability.

Among the examined structural parameters, only the correlation between the $\log f H_2O$ and the parameters listed in Table 1.4 appears to be significant. Applying Brown and Shannon's curve (1973), the bond strengths were

Figure 1.4 The LogfH_2O versus 1/T (K) plot for different synthetic amphiboles (modified from Wones, 1981).
Abbreviations used:

FTr, ferrotremolite, Ernst, 1966	Tr, tremolite, Boyd, 1959
Fpa, ferropargasite, Gilbert, 1966	Pa, pargasite, Boyd, 1959
FRi, ferrorichterite, Charles, 1975	Ri, richterite, Charles, 1975
Ha, hastingsite, Thomas, 1977	Gr, grunerite, Forbes, 1977

MHa, Magnesiohastingsite, Semet & Ernst, 1981
An, Anthophyllite, Chernosky & Auto, 1979
Rb-Arf, riebeckite-arfvedsonite, Ernst, 1962
MRb, magnesioriebeckite, Ernst, 1960

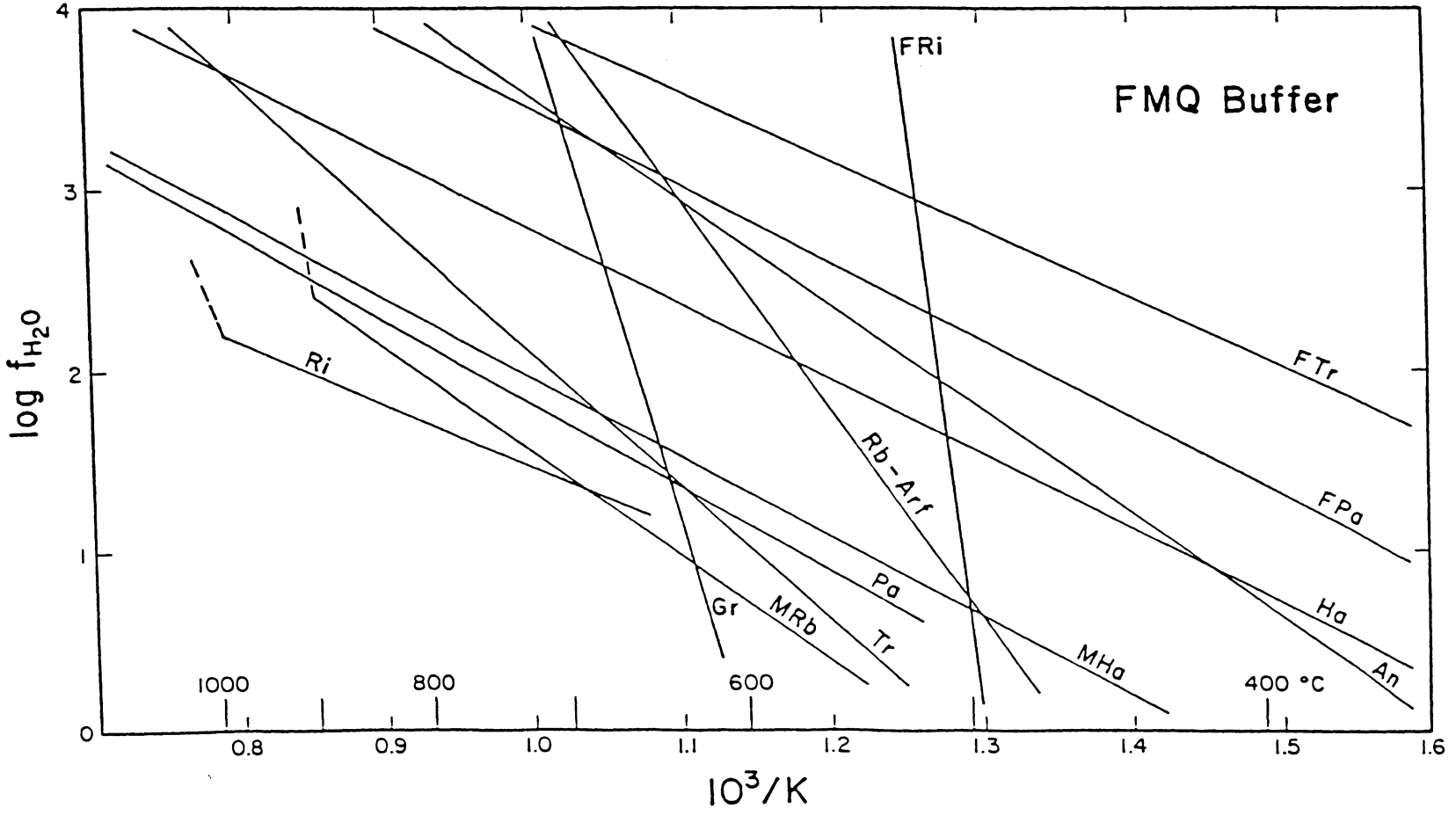
FMQ Buffer
FRi
FTr
FPa
Ha
An
MHa
Rb-Arf
Pa
Tr
MRb
Gr
Ri
log f_{H_2O}
$10^3/K$
1000
800
600
400 °C
0.8
0.9
1.0
1.1
1.2
1.3
1.4
1.5
1.6
0
1
2
3
4

Table 1.3 Cell parameters for natural and synthetic amphiboles

Mineral	*a*	*b*	*c*	*β*	Reference
Mg-Riebeckite	9.890	17.950	5.310	72.50	Whittaker, 1949
Mg-Riebeckite*	10.040	18.020	5.280	72.00	Ernst, 1960
K-Arfvedsonite	9.935	18.102	5.339	103.90	Litvin *et al.*, 1976
Arfvedsonite *	9.760	18.060	5.340	103.40	Ernst, 1962
Tremolite	9.863	18.048	5.285	104.79	Hawthorne & Grundy, 1976
Tremolite *	9.833	18.054	5.268	104.52	Boyd, 1959
Actinolite	9.891	18.200	5.305	104.64	Mitchell *et al.*, 1971
Actinolite *	9.970	18.340	5.300	104.50	Ernst, 1966
Grunerite	9.564	18.393	5.339	101.89	Finger, 1969
Grunerite *	9.572	18.450	5.344	101.55	Forbes, 1977
Pargasite	9.851	17.981	5.293	105.07	Bocchio *et al.*, 1978
Pargasite *	9.870	18.006	5.300	105.26	Boyd, 1959
Mg-Hastingsite	9.848	17.974	5.299	105.06	Bocchio *et al.*, 1978
Mg-Hastingsite *	9.933	18.029	5.293	105.43	Semet, 1981
Hastingsite	9.945	18.239	5.340	104.95	Litvin, 1973
Hastingsite *	9.997	18.179	5.323	105.34	Thomas, 1982
Na-Richterite	9.824	17.968	5.263	104.22	Cameron & Gibbs, 1971
Na-Richterite *	9.902	17.980	5.269	104.22	Charles, 1974
Fe-Na-Richterite	9.846	18.019	5.274	104.25	Cameron & Gibbs, 1971
Fe-Richterite *	9.982	18.223	5.298	109.73	Charles, 1974

* Synthetic phase.

Table 1.4 Pearson correlation coefficient between some structural parameters and $\log fH_2O$ at different temperatures (°C)

Parameter	600	700	800
T(2)O	-0.53	-0.82	-0.85
OO(T2)	-0.53	-0.79	-0.80
T(1)O(5)T(2)	0.59	0.91	0.93
T(1)O(6)T(2)	0.61	0.85	0.84
T(1)O(7)T(1)	0.71	0.91	0.89
M(1)O	0.75	0.75	0.67
M(3)O	0.48	0.64	0.62
M(1)M(3)	0.69	0.73	0.66
M(2)M(3)	0.74	0.91	0.87

calculated for all the octahedral sites. For the M(1) and M(3) sites, the calculated bond strengths, which depend on the bond lengths and site occupancies of an individual structure, also correlate with the $\log fH_2O$ ($R \approx 0.6$). Similar results were obtained from electrostatic potential energy calculations, using the FORTRAN program ELEN2 (Ohashi and Burnham, 1972; Ohashi, 1976). The bond overlap population, obtained from EHMO calculation, is essentially constant, for the same cation, regardless of the geometry. Cameron (1970) also obtained constant energy for the same cation. The long Fe-O bonds have a low bond overlap population, which is consistent with data reported by Cameron and Gibbs (1973).

The low correlations between each of the structural parameters and stability and between the calculated potential energies and stability appear to be a consequence of the natural samples not having the end-member compositions. However, the bonding parameters of the cations in the M(1) and M(3) sites consistently show a higher correlation with the water fugacity than those of the cations in the M(2) and M(4) sites. This reflects the dehydration nature of the amphibole break-down reaction, since the OH is bonded to the M(1) and M(3) cations. It is, however, difficult if not impossible to determine the hydrogen positions accurately by conventional *x*-ray structure refinement and to determine the OH occupancy by analytical methods. Thus, the OH bond length, bond strength and occupancy cannot be obtained from *x*-ray structure analyses.

Infrared absorption spectra of amphiboles show the fine structure of the hydroxyl group. The frequency of the absorption band is related directly to the strength of the OH bond. Thus, infrared spectra of amphiboles, both natural and synthetic, have been measured to establish a connection between OH

bond strength and the thermal stability of amphiboles; in addition, two natural grunerites NMNH No. R7702 and NMNH No. R16782 have been studied hydrothermally to determine their decomposition temperatures at 1, 2 and 3 kbar and to compare these data with earlier studies (Forbes, 1977 and Fonarev *et al.*, 1976; 1977a, b, c; 1979; 1980); and the crystal structure of grunerite Klein No. 9A has been refined and compared with grunerite Klein No. 1 (Finger, 1969) and cummingtonite (Ghose, 1961; Fisher, 1966) in order to verify the structural changes with various Fe⇔Mg substitution.

CHAPTER 2. THE INFRARED HYDROXYL BAND AND THERMAL STABILITY OF AMPHIBOLE

Introduction

Attempts to establish correlations between structural parameters and thermal stability of amphiboles, Chyi and others (1982) showed that the bonding of the cations in M(1) and M(3) sites seems to exert a greater control on the thermal stability than that of the M(2) and M(4) cations. This is thought to reflect the dehydration nature of the amphibole break-down reactions, since the OH is bonded to the cations in both M(1) and M(3). Infrared absorption spectra of amphiboles show the fine structure of the hydroxyl group. The frequency of the absorption band is directly related to the strength of the OH bond. Infrared spectra of different amphiboles, both natural and synthetic, were examined and correlated to thermal stability data.

Hydroxyl Stretching Frequency and Thermal Stability

High-resolution infrared absorption spectra of minerals containing brucite-like layers commonly show the fine structure of the hydroxyl groups . This structure was first noted by Vedder (1964) in natural talc. He observed four distinguishable bands in mixed (Fe, Mg) talc and assigned them to hydroxyl groups linked to 3Mg, 2Mg+Fe, Mg+2Fe, and 3Fe ions. Four similar bands, observed in spectra of Fe-Mg binary clinoamphiboles (Burns and Strens , 1966), were designated as the A, B, C, and D bands, respectively. In the clinoamphibole structure, the hydroxyl is bonded to two symmetrically equivalent M(1) cations and one M(3) cation. End-member amphiboles with

only one type of cation in these three sites have a single sharp hydroxyl stretching band (A or D), whereas amphiboles with intermediate compositions show different combinations of all four bands.

The relative intensities of these bands differ with composition, but their relative positions are constant within the individual binary systems (Burns and Strens, 1966; Strens, 1966; Wilkins, 1970). The intensity of an absorption band, which results from the transition of the system from some initial energy level to a final energy level, depends on the population at the initial energy level. Burns and Strens (1966) used this principle to develop a technique for site population estimates for amphiboles.

Vibrational frequency depends on the force constant, atomic mass, and the structure. High stretching frequencies are associated with strong bonds. Accordingly, the higher stretching frequencies associated with MgMgMg-bonded, as compared to FeFeFe-bonded, OH indicate that a weaker OH bond results when Fe replaces Mg. Burns and Strens (1966) thought that this substitution strengthens the metal-oxygen bonds and hence weakens the hydrogen-oxygen bonds. The infrared spectra of heated crocidolite and glaucophane (Patterson and O'Connor, 1960; Ernst and Wai, 1970) showed that the OH bonded to Fe^{+2} was lost before the OH bonded to Mg was lost. Hydrothermal studies have also demonstrated a systematically higher thermal stability of Mg end-members as compared to their Fe-analogues (Boyd, 1959; Ernst, 1966; Gilbert, 1966; Charles, 1975; Thomas, 1977, 1982; and Semet and Ernst, 1981) (Figure 2.1).

Using the data of Burnham *et al.* (1969) for the properties of water and taking all these reactions to be equilibria involving only pure solids and purewater, the stability curves are plotted, as a function of $\log f H_2O$ and

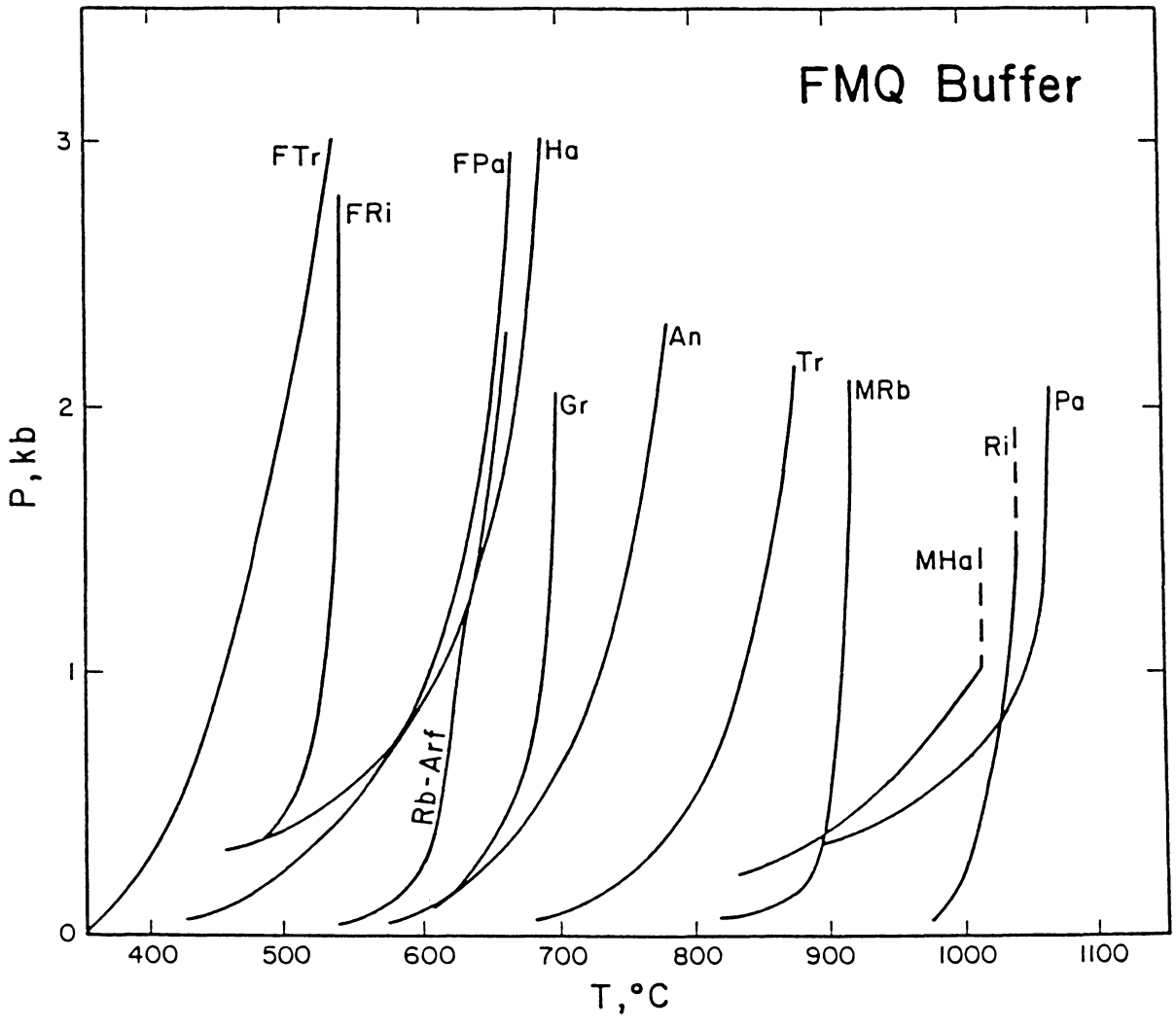

Figure 2.1 Upper thermal stability of several Mg-Fe amphibole pairs.
(Abbreviations are the same as in Figure 1.4)

1/T(K) at 1 atm (See Figure 1.4). The $\log f H_2O$ value for amphibole decomposition reactions was calculated from experimental data. Where possible, reactions under fayalite-magnetite-quartz (FMQ) buffer conditions were chosen. The stability field of each phase is to the low temperature side of its corresponding curve. Thus, at 1 atm pressure and a constant temperature, phases with lower minimum $\log f H_2O$ values are the more stable phases. The hydroxyl 'A' band observed for natural samples was assigned as the hydroxyl frequency of the synthetic Mg end-member and the 'D' band was assigned as that of the synthetic Fe end-member. Figure 2.2 shows scatter diagrams of OH frequency versus $\log f H_2O$ at different temperatures and exhibits a significant negative correlation (R = -0.33 at 600°C , R = -0.87 at 700, R = -0.90 at 800°C). Phases with low $\log f H_2O$ values have stronger OH bonds. In other words, a stronger O-H bond is associated with the more stable phase assuming all other things being equal. This suggests that the strength of the OH bond may be the key to understanding the thermal stability of amphiboles. Note, however, that grunerite and magnesioriebeckite are outliers.

Gilbert and others (1982) pointed out that the thermal stability of synthetic grunerite (Forbes, 1977) is inconsistent with the thermal relations obtained by Fonarev and his coworkers (1976; 1977; 1979a, b; 1980). However, the correlation that is shown in Figure 2.2 needs to be verified with hydroxyl stretching bands obtained for synthetic samples.

Experiments

The infrared absorption spectra of finely powdered synthetic riebeckite-

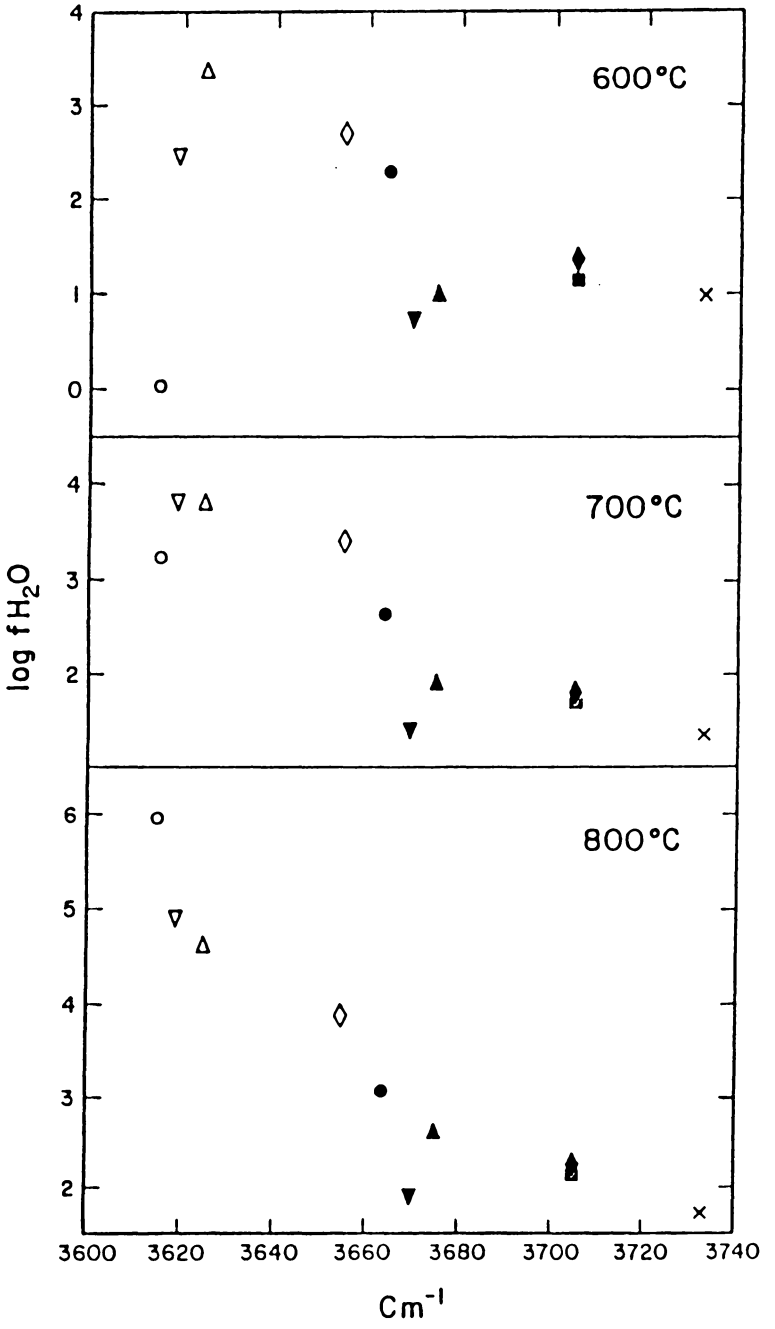

Figure 2.2 LogfH_2O versus OH stretching frequency at different temperatures.
Symbols used:
O grunerite ● anthophyllite Δ ferrotremolite
▲ tremolite × richterite ■ pargasite
◊ hastingsite ♦ magnesiohastingsite
▽ riebeckite-arfvedsonite ▼ magnesioriebeckite

arfvedsonite, magnesio-riebeckite, pargasite-ferroparagasite, and richterite-ferrorichterite and eighteen natural cummingtonite-grunerite samples, obtained from the Smithsonian Institution, embedded in KBr pellets have been recorded by means of a Nicolet MX-1 Fourier Transform Infrared Spectrophotometer with 1 cm^{-1} resolution. Pressed pellets of the materials were kept at 120°C for more than one week in an attempt to remove adsorbed molecular water, and then kept in a vacuum desiccator prior to recording their spectra. Nonetheless, some samples still contained traces adsorbed water, that gave rise to a broad absorption band near 3550 cm^{-1} and another absorption band around 1650 cm^{-1}, the region that represents deformation vibration of water (Lazarev, 1972). Chemical analyses of these eighteen natural samples were obtained with an ARL electron microprobe using 15 kV operating voltage and 20 nanoamps beam current. Corrections for atomic number, fluorescence, and absorption were made with the Bence-Albee program (1968). (See Appendix A).

The Hydroxyl Group of Synthetic Amphiboles

Riebeckite-Arfvedsonite and Magnesioriebeckite series

The IR spectra of the hydroxyl group of the three synthetic riebeckite-arfvedsonite samples and one natural sample of arfvedsonite, NMNH #48224, are shown in Figure 2.3a. Multiple absorption bands observed for the sample WR-44 (synthesized under WM buffer conditions) suggest that cations other than Fe^{+2} are in the M(1) and M(3) sites. Reported site occupancies of natural riebeckitic-arfvedsonitic amphiboles differ from study to study.

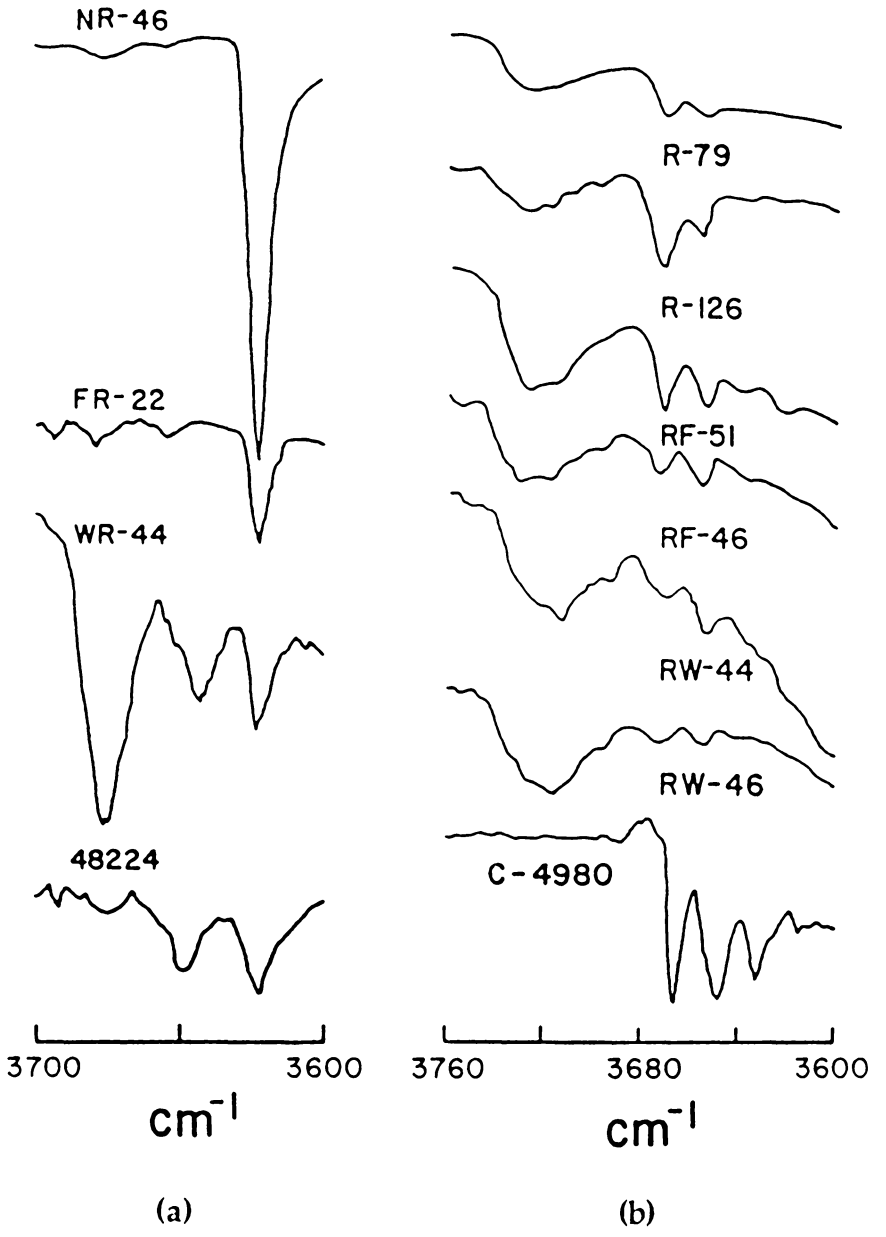

Figure 2.3 Hydroxyl group of (a) riebeckite-arfvedsonite and (b) magnesioriebeckite.

Litvin *et al.* (1976) assigned the Fe^{+2} and Fe^{+3} to the M(1) and M(3) sites by comparing the *x*-ray and Mössbauer data. He also suggested that Na is ordered into the M(3) site in a potassium arfvedsonite sample. Hawthorne (1976) found only Fe^{+2}, Mn, and Mg in the M(1) and M(3) sites in his structural analysis of a potassium arfvedsonite. The presence of Fe^{+3} in the M(1) and M(3) sites has been suggested from Mössbauer spectral and infrared spectral studies (Burns and Prentice, 1968; Bancroft and Burns, 1969; Ernst and Wai, 1970; and Burns and Greaves, 1971). The spectrum of sample WR-44 suggests that cations other than Fe^{+2} are present at the M(1) and M(3) sites. The bands occurring at higher frequencies cannot be attributed completely to Fe^{+3} occupancy of the M(1) and M(3) sites because it has been found in natural samples that the $Fe^{+2}Fe^{+2}Fe^{+2}$-bonded OH has a higher frequency than the OHs bonded to $Fe^{+2}Fe^{+2}Fe^{+3}$, $Fe^{+2}Fe^{+3}Fe^{+3}$ and $Fe^{+3}Fe^{+3}Fe^{+3}$ (Table 2.1). However, when a monovalent cation, M, such as Li or maybe Na occupies the M(1) or M(3) site, the $M^{+}Fe^{+2}Fe^{+2}$ and $M^{+}Fe^{+2}Fe^{+3}$-bonded OH has a higher stretching frequency than the $Fe^{+2}Fe^{+2}Fe^{+2}$-bonded OH. A higher stretching frequency could also result from the Na-occupied A site (Rowbotham and Farmer, 1973).

A single sharp band at 3622 cm^{-1} for samples NR-46 (Ni-NiO buffer) and FR-12 suggests that the samples have Fe^{+3} ordered into the M(2) sites. The band position, also consistent with that observed in natural samples (3619 cm^{-1}, Burns and Prentice, 1968; Strens, 1974), is assigned as D ($Fe^{+2}Fe^{+2}Fe^{+2}$) band. This may indicate that these two samples are of near riebeckite end-member composition.

The hydroxyl groups of six synthetic $Na_2Mg_3Fe_2^{+3}Si_8O_{22}(OH)_2$, magnesio-riebeckite, samples and one natural sample C-4980 (from Ernst and Wai, 1970)

Table 2.1 Frequency shift of the principle OH stretching band relative to the A band
(from Hawthorne, 1983)

Band	Configuration	Displacement
A	MgMgMg	0
B	$MgMgFe^{+2}$	-14
C	$MgFe^{+2}Fe^{+2}$	-27
D	$Fe^{+2}Fe^{+2}Fe^{+2}$	-47
E	$MgMgFe^{+3}$	-22
F	$MgFe^{+2}Fe^{+3}$	-36
G	$MgFe^{+3}Fe^{+3}$	-44
H	$Fe^{+2}Fe^{+2}Fe^{+3}$	-51
I	$Fe^{+2}Fe^{+3}Fe^{+3}$	-58
J	$Fe^{+3}Fe^{+3}Fe^{+3}$	-66
K	MgMgAl	-9
L	$MgFe^{+2}Al$	-22
M	$Fe^{+2}Fe^{+2}Al$	-38
N	MgAlAl	-
O	$Fe^{+2}AlAl$	-38
P	$MgFe^{+3}Al$	-
Q	$Fe^{+2}Fe^{+3}Al$	-
-	$LiFe^{+2}Fe^{+2}$	-27
-	$LiFe^{+2}Fe^{+3}$	-34
-	$LiMgFe^{+3}$	-20
-	Na at A	+24
-	K at A	+31
-	Al for Si	-75
-	Ti at M(1,2,3)	-87, -99
-	Ca at M(4)	$+2n, 0<n<4$

are shown in Figure 2.3b. The high frequency OH-stretching band observed in the synthetic $Na_2Mg_3Fe_2^{+3}Si_8O_{22}(OH)_2$ samples may also result from an occupied A site (Rowbotham and Farmer, 1973). The four bands observed for natural samples (Burns and Prentice, 1968) also appear in the spectra of synthetic $Na_2Mg_3Fe_2^{+3}Si_8O_{22}(OH)_2$ samples. The presence of the four bands indicates the presence of Fe^{+2} in the M(1) and M(3) sites. These observations indicate that the synthetic samples have different cation ordering schemes as compared to the ordering in the natural samples and that the synthetic samples have variable $Fe^{+3}/(Fe^{+2} + Fe^{+3})$ ratios and thus are not end-member compositions. This is also indicated by the refractive index measurements of the synthetic samples made by Ernst (1962).

Richterite-Ferrorichterite Series

The bands for the hydroxyl groups of the synthetic richterite-ferrorichterite series, which are at 3733, 3714, 3702, and 3681 cm^{-1}, are assigned as A, B, C and D bands, respectively (Figure 2.4a). The presence of ferroactinolite is suggested by the bands at 3625, 3650, and 3675 cm^{-1} (Rowbotham and Farmer, 1973). The hydroxyl stretching frequencies of a natural richterite NMNH #143158 were different from those of synthetic samples. The 3733 cm^{-1} band is consistent with the 3731 cm^{-1} band observed by Mottana and Griffin (1986) for two K-richterites from St. Marcel, Italy. They also observed a strong absorption band at 3715 cm^{-1}, which they assigned to the Sr-MgMgMg-OH band based on the chemical analyses of the samples; they assigned Sr to the A site. The synthetic ferrorichterite, without Sr, also has a band at 3714 cm^{-1}. Thus, the 3715 band can also be interpreted as MgMgMn bonded OH with an

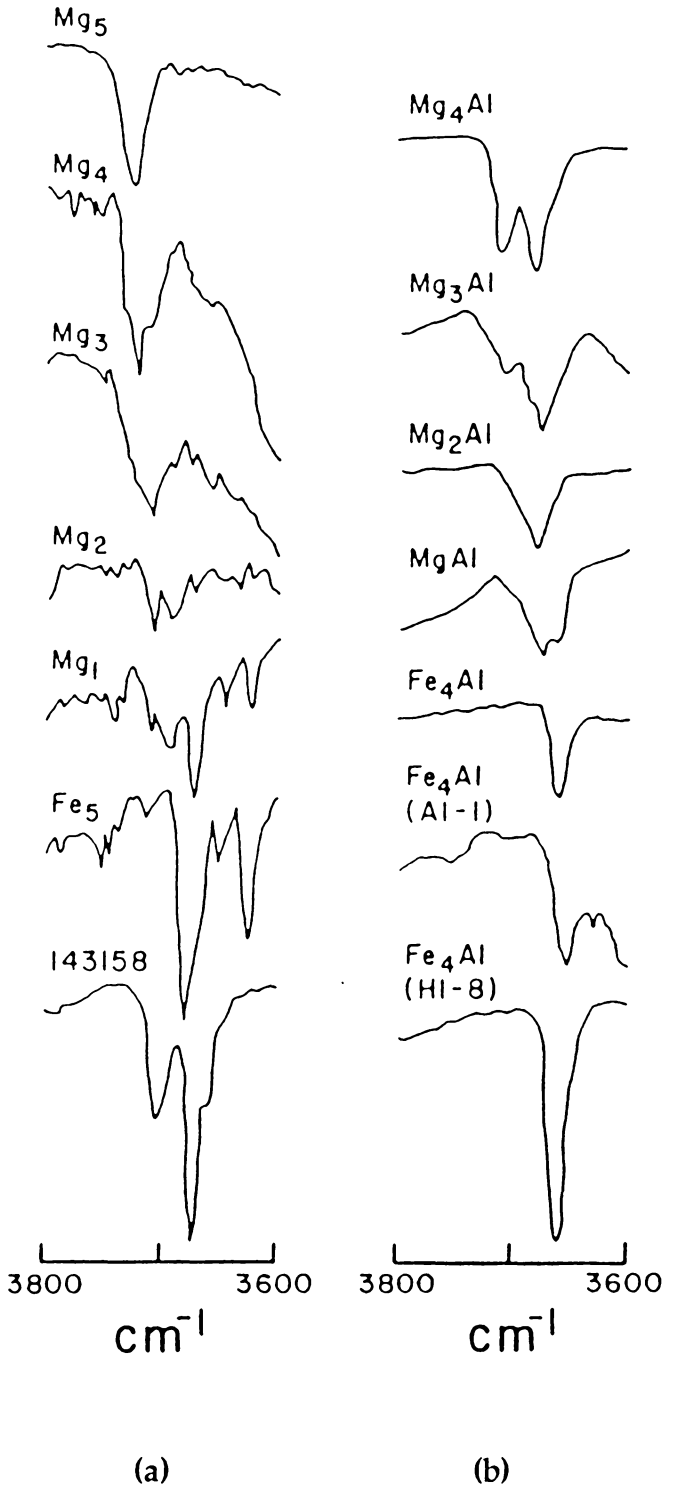

Figure 2.4 Hydroxyl group of (a) richterite-ferrorichterite and (b) pargasite-ferropargasite series.

occupied A site. Since Mn behaves in the same manner as Fe, the frequency shift between MgMgMg bonded and MgMgFe bonded OH is about 14 cm^{-1} (See Table 2.1), whereas the observed frequency difference is 16 cm^{-1}. Furthermore, according to the reported analyses, the sample has 0.071 Mn per formula unit (pfu) and 0.051 Sr pfu.

The greater thermal stability of compositions Mg_5 through Mg_2Fe_3 compared to $MgFe_4$ and Fe_5 pointed out by Charles (1975) also correlates with the presence of a high frequency hydroxyl stretching band (Figure 2.4a).

Ferropargasite-Pargasite series

Semet (1973) found that Al is distributed randomly over M(1), M(2) and M(3) sites in synthetic pargasite rather than ordered into the M(2) site as determined from the structural and chemical analyses of natural samples (Robinson *et al.*, 1973; Bocchio *et al.*, 1978)

The IR spectra of the hydroxyl group of synthetic pargasite-ferropargasite of Charles (1977) and ferropargasite of Gilbert (1966) suggests further that Al is distributed randomly through M(1), M(2) and M(3) sites in synthetic samples only when Mg is present (Figure 2.4b). A single sharp band for the synthetic ferropargasites indicates that Al is ordered into the M(2) site. Makino and Tomita (1986) examined five natural hornblendes of metamorphic or volcanic origin. On the basis of the mean M-O bond lengths from least-squares refinements, they concluded that the Al and Fe^{+3} ordered to the M(2) site at low formation temperatures.

An additional band at 3685 cm^{-1} is present whenever Fe is introduced into the system; the frequency shifted down about 27 cm^{-1} (from 3712 to 3685),

which suggests a cation configuration of MgFeFe (See Table 2.1). A slight down shift (from 3680 to 3678cm^{-1}) of the presumably AlAlAl-bonded OH band also occurs when Fe is introduced into the system. The frequency shift between MgMgMg-bonded OH and FeFeFe-bonded OH (3660 cm^{-1}) for this series is 52 cm^{-1}.

The Infrared Spectra of Fe-Mg-Mn Amphiboles

The hydroxyl frequencies of these samples are plotted in Fig 2.5. The Mn is combined with Fe since Mn behaves in the same manner as Fe and no additional band occurs because of its presence.

The relative intensities of the A, B, C and D bands vary directly with chemical composition. The most intense band switches from A for Mg-rich, to B and C for intermediate compositions, to D for the Fe-rich grunerite. Burns and Strens (1966) observed the shift of the OH bands to higher frequencies for an Mn-cummingtonite and concluded that it resulted from the large Mn in the M(4) site. Bancroft *et al.* (1967) examined the Mössbauer spectrum of a high Mn-cummingtonite (23.7 mole % Mn) and suggested that Mn preferentially occupies the M(4) site but that Mn also enters the M(1) and M(3) sites. The spectrum was, in addition, reported to be of poor quality. From an examination of a linear combination of the mean M-O distances from 'ordered' end-members, Papike *et al.* (1969) suggested that the M(4) site is preferred by Mn in the Mn-cummingtonite structure. Maresch and Czank (1983) have since investigated synthetic amphiboles on the join $Mn_x^{2+}Mg_{7-x}Si_8O_{22}(OH)_2$ and found that not only the symmetry but also an abundance of multiple chain combinations and stacking faults in the structure differ from

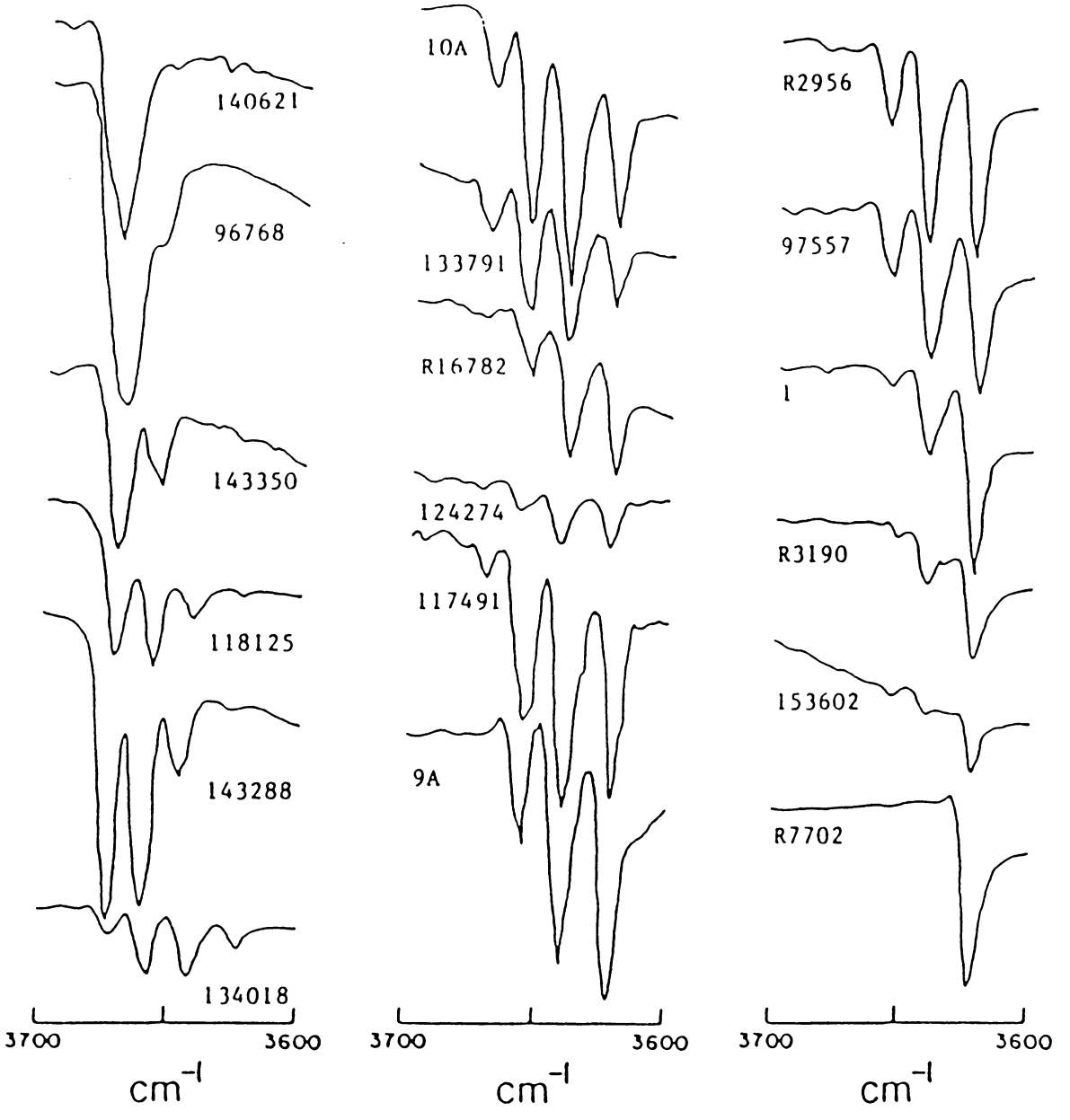

Figure 2.5 Hydroxyl stretching frequencies of Fe-Mg amphiboles.
(Fe+Mn/Fe+Mn+Mg ratio increases from top left to bottom right)

those of the natural analogue. They suggested that the Mn^{+2} was probably disordered into octahedral sites. A study of the hydroxyl stretching bands of these synthetic $Mn_x^{2+}Mg_{7-x}Si_8O_{22}(OH)_2$ specimens is needed in order to examine the Mn ordering in synthetic "biopyriboles". The shifting of the OH bands was also observed for high Mn samples. However, the relative intensities of the three samples with high Mn content NMNH #140621, #143288 and #124274 fall in the trend of increasing (Fe+Mn)/(Fe+Mn+Mg) ratio. This suggests that Mn enters the M(1) and M(3) sites, contributes part of of the band intensities, and causes the band shifting to higher frequencies. It also suggests that linear combination of mean M-O distances is inadequate even to approximate the site occupancy.

Discussion

The hydroxyl stretching frequency of amphiboles varies with M(4) site and A site occupancies. Calcic amphiboles, with Ca in the M(4) site, persist at higher temperatures than the Fe-Mg analogues. They are represented by the end-member pairs tremolite and anthopyllite, and ferrotremolite and grunerite. The MgMgMg-OH frequency for tremolite (3675 cm^{-1}, Wilkin, 1970) is higher than that for anthophyllite (3661 cm^{-1}, Burns and Law, 1970). Charles (1975) pointed out that the substitution of $Na^{A}Na^{M(4)} \rightarrow Ca$, which fills the vacant A site, greatly stabilizes the resulting richterite. Occupancy of the A site increases the OH stretching frequencies (Rowbotham and Farmer, 1973), which correlates with the high thermal stability of A site occupied amphiboles. The variation of the hydroxyl stretching frequency seems to be consistent with the presently used classification scheme of amphiboles on the

basis of M(4) cation occupancy (Leake, 1978).

Strens (1974) correlated the OH band frequency with the electronegativity of the cations bonded to the hydroxyl group. Strengthening of the metal-oxygen bonds as Fe replaces Mg in the clinoamphibole structure, as suggested by Burns and Strens (1966), is inconsistent with the high melting temperature observed for Mg end-members in Fe-Mg binary systems such as those of the olivines and the pyroxenes. Burns and Strens (1966) suggested that the high hydroxyl stretching frequencies of the tremolite-actinolite series may result from compression of the Si_6O_{18} ring when (Fe,Mg) in the M(4) site is replaced by the larger Ca cation. Accordingly, they assigned the Mn to the M(4) site in Mn-cummingtonite to explain the shifting of hydroxyl frequencies. Maresch and Czank (1983) suggested that the Mn^{+2} was probably disordered into octahedral sites in the synthetic $Mn_x^{2+}Mg_{7-x}Si_8O_{22}(OH)_2$ samples.

The arfvedsonite, synthesized under Ni-NiO buffer (NR-46), has a single sharp hydroxyl band at 3622 cm^{-1}. The calculated $\log f H_2O$ for arfvedsonite stability curve under Ni-NiO buffer at 600, 700, and 800°C were 2.83, 3.77, and 4.53, respectively. The correlation coefficient between the $\log f H_2O$ and the hydroxyl stretching frequency are -0.33, -0.85, and -0.89 for 600, 700, and 800°C, respectively (Figure 2.6).

The presence of a high hydroxyl stretching frequency in the spectra of synthetic magnesioriebeckite indicates that a stronger OH bond and a higher thermal stability is to be expected for the synthetic samples than for the natural specimens. This suggests that under the same buffer condition and at the same temperature the $\log f H_2O$ for a natural sample should be higher (less stable). Either increasing the stretching frequency or the water fugacity for the magnesioriebeckite point on Figures 2.6 improves the correlation. This

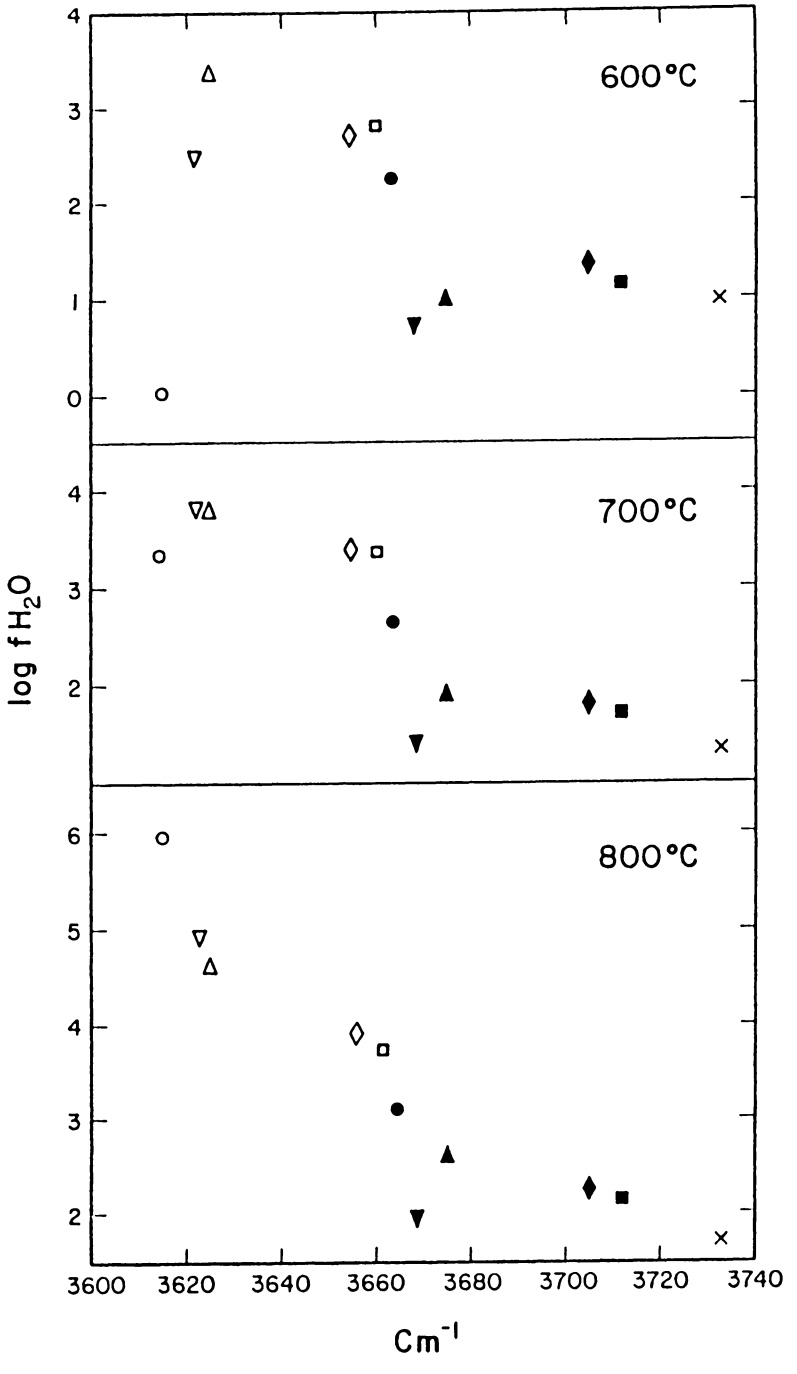

Figure 2.6 LogfH_2O versus OH stretching frequency at different temperatures.
(Symbols are the same as in Figure 2.2)

clearly indicates that the strength of the OH bond may be the key to understanding the thermal stability of amphiboles. The frequency difference between MgMgMg-bonded OH and FeFeFe-bonded OH is nearly constant (about 47 cm^{-1}), which may explain the regularity in the thermal stability spread (about 400°C) between Fe and Mg end-members.

Heating experiments (Barnes, 1930; Addison *et al.*, 1962a, b; Hodgson *et al.*, 1965; Gibb and Greenwood, 1965; Littler and Williams, 1965; Patterson, 1965; Patterson and O'Connor, 1966; Freeman, 1966; Clark and Freeman, 1967; Vedder and Wilkins, 1969; Ernst and Wai, 1970), indicate a loss of the proton H^+ and the simultaneous oxidization of Fe^{+2} to Fe^{+3} to maintain the charge balance and structural integrity during the early stages of heating. Once all the protons are lost, further oxidization of Fe^{+2} will induce charge imbalance and lead to collapse of the structure. Thus, in an Fe-Mg binary system, samples with more Fe^{+2} will decompose at lower temperatures.

The differences among the infrared spectra of synthetic and natural samples suggests the following:

1. The cation ordering in synthetic samples differs from that observed in natural samples; the observed differences may, however, reflect the need for more precise structural refinements of both the natural and the synthetic samples.
2. Some synthetic amphiboles do not have end-member compositions; therefore, experimental studies must include detailed analyses of the resultant phases. Even then, stability studies of synthetic minerals should be applied to natural systems with great caution.
3. The conventional method of identifying run products by *x*-ray diffraction is not sufficient; high resolution transmission electron

microscopy (TEM) and infrared spectra, which may reveal the microstructure of the minerals, are also needed.

4. Studies of the cation ordering of synthetic amphiboles using infrared and Mössbauer spectroscopy should be made and compared with results obtained for natural samples; these studies may help delineate the chemical and physical conditions that existed when the amphiboles were formed.

CHAPTER 3. THE UPPER THERMAL STABILITY OF GRUNERITES

Introduction

The thermal stability of grunerite reported by Forbes (1977) was established by optical detection of the increase or decrease in the amount of amphiboles over an initial 1.5% seeding, with only a maximum of 10 percent amphibole being reported. Fonarev and co-workers (Fonarev *et al.*, 1976; 1977; 1979a, b; 1980) examined the stability of cummingtonite-grunerite series under the fO_2 defined by FMQ buffer. Gilbert and others (1982) compiled the experimental data from Fonarev and co-workers (Figure 3.1) and pointed out the inconsistency between the extrapolated thermal stability of pure grunerite end-member at 2940 bars and Forbes' data (1977). They also pointed out that on the basis of comparing the thermal stability of several Fe-Mg amphibole pairs (See Figure 2.1) the thermal stability determined by Forbes for pure grunerite seems to be too high.

Difficulties in synthesis of the pure Fe end-member were noted by earlier workers (Smith, 1957; Greenwood, 1963; Forbes, 1971) and attempts to synthesize grunerite from oxide mixes were unsuccessful. This study of the upper thermal stability of natural grunerite under FMQ buffer was initiated in order to resolve the earlier inconsistances.

Experiments

Conventional Rene 41 externally heated cold-seal pressure vessels (Tuttle, 1949) were used in this investigation. Temperatures were measured

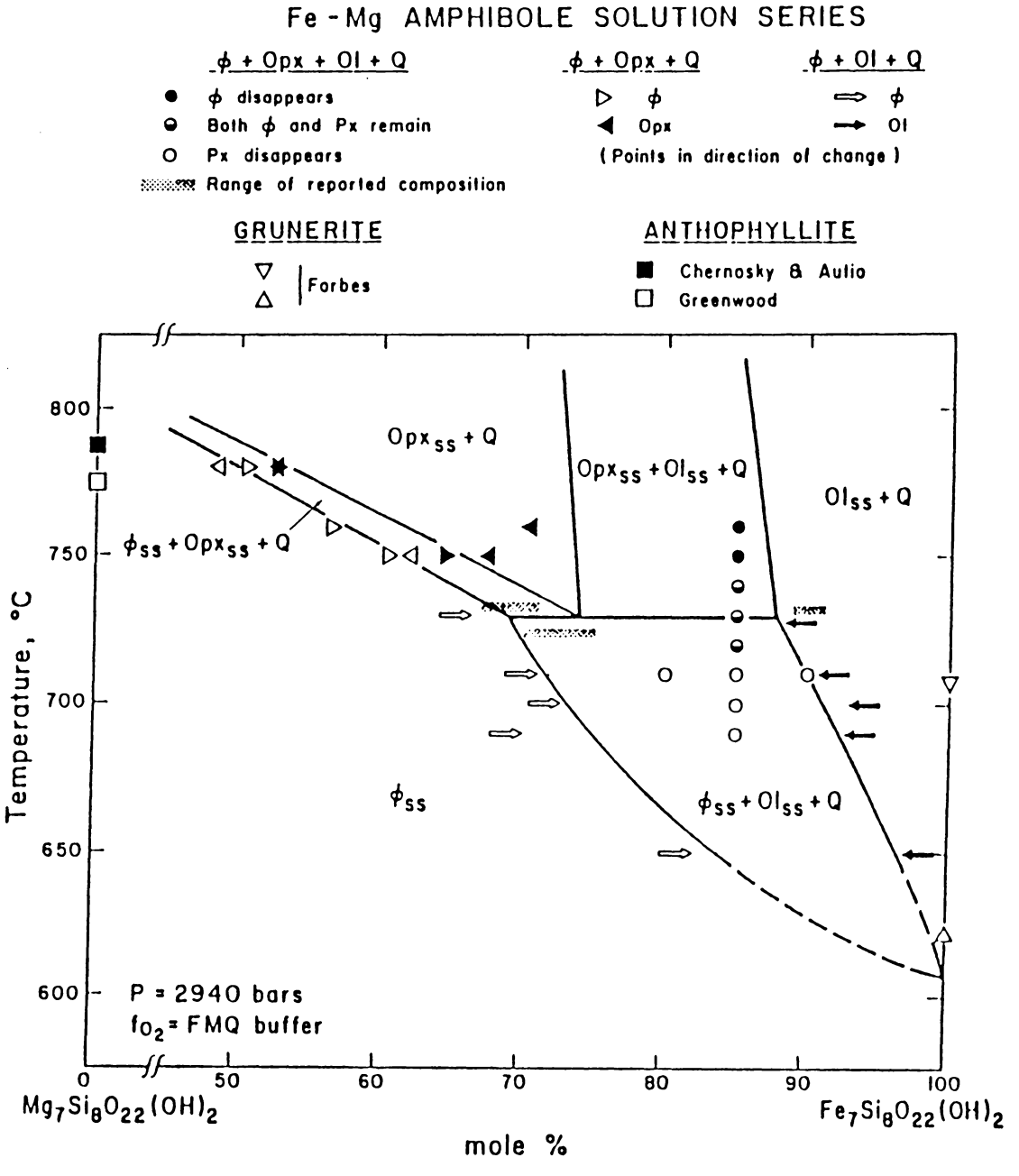

Figure 3.1 T-X section on the Mg_7-Fe_7 join at 2940 bar.
(from Gilbert *et al.*, 1982)

with external chromel-alumel thermocouples. Solid state temperature controlers (Hadidiacos, 1969) were used, and temperature fluctuations of no more than ±3°C were observed. Several thermocouple-pressure vessel assemblies were calibrated against the melting point of NaCl (800.4°C) and LiCl (605°C) and the measured temperatures were within ±3°C. The total water pressure was measured by a Heise Bourdon gauge and is believed to have been accurate within ± 50 bars.

All runs were brought to temperature and quenched isobarically. Runs were quenched by passing a stream of compressed air over the pressure vessels after removal from the furnaces. Oxygen fugacities were controlled by a fayalite-magnetite-quartz buffer (Hewitt, 1978), utilizing the double capsule technique described in Eugster and Wones (1962).

Starting materials for runs consisted of: (1) amphiboles: two natural samples obtained from the National Museum of Natural History (NMNH # R16782 and #R7702) and (2) fayalite + quartz + 3-5% natural amphiboles.

The run conditions and durations are shown in Tables 3.1 and 3.2. All runs were checked for the presence of H_2O in the inner and outer capsules when they were opened. All buffers were checked by either optical or *x*-ray methods.

Phase Identification

The phases in the run charges as well as in the buffers were examined optically and/or by microprobe analyses. The cell dimensions of the run charges were determined from *x* -ray powder diffraction patterns recorded with a Norelco (Ni-filtered Cu$K\alpha$ radiation) diffractometer equipped with

Table 3.1 Experimental results for grunerite NMNH#R7702

Run No.	Starting Material	Temp. (°C)	Pressure (bar)	Duration (days)	Run Products
10	G	622	3000	108	G
4	G	627	3000	31	F+M+Q+(G)**
6	G	628	3000	110	F+M+Q+G
2	G	642	3000	33	$F_{0.999}$+M+Q
5	G	622	2000	49	G+F+Q+(M)
12	G	622	2000	30	G+F+Q
13	G	622	2000	30	$G_{0.999}$+F+Q
20	G+F+Q	625	2000	15	F+Q+M+(G)
11	G	628	2000	20	F+Q+M+(G)
16	G	632	2000	20	F+Q+M
18	G	612	1250	7	$G_{0.999}$+Q+(F)
17	G	622	1250	7	F+Q+M+(G)
21	G	624	1250	9	F+Q+M
19	G	630	1000	10	F+Q+M

Abbreviations used: G, grunerite; F, fayalite; Q, quartz; M, magnetite;

* Fe/(Fe+Mg) ratio.

**Phase in parentheses is in trace amount.

Table 3.2 Experimental results for grunerite NMNH #R16782

Run No.	Starting Material	Temp. (°C)	Pressure (bar)	Duration (days)	Run Products
6	G	730	3000	16	$G_{0.706-0.710*}$+(Opx+Q)**
10	G	735	3000	30	$G_{0.707}$+$Opx_{0.711-0.744}$+Q
7	G	775	3000	16	$Opx_{0.700}$+Q+(F)
9	G	675	2000	30	$G_{0.705-0.712}$
16a	G	692	2000	20	G
16b	G+F+Q	692	2000	20	G+F+Q+(M)
14a	G	732	2000	20	G+Opx+Q
14b	G+F+Q	732	2000	20	G+F+Q+$Opx_{0.711}$
1	G	672	1000	70	G
15a	G	720	1000	20	$G_{0.705-0.709}$+(Opx)
15b	G+F+Q	720	1000	20	G+F+Q+(M+Opx)
17	G	725	1000	10	G+Opx+Q
18	G	730	1000	10	G+Opx+Q

Abbreviations used: G, grunerite; F, fayalite; Q, quartz; M, magnetite; Opx, orthopyroxene.

* Fe/(Fe+Mg) ratio.

** Phase (Phases) in parentheses is (are) in trace amount.

a graphite monochromator. CaF_2 (a = 5.4632 Å) was used as an internal standard. The least-squares refinement of the cell parameters were obtained using the program of Burnham (1986, IBM PC version). Chemical analyses were obtained with an ARL-SEMQ electron microprobe using 15 kV operating voltage and 20 nanoamps beam current. Corrections for matrix effects were made with the Bence-Albee program (1968). The resulting phase assemblages are given in Tables 3.1 and 3.2.

Results

The experimental results for Fe-rich grunerite (R7702) suggest a decomposition reaction of:

Fe-rich grunerite ⇒ olivine + quartz + magnetite + vapor.

Euhedral quartz crystals, which nucleated on the surface of grunerite (Figure 3.2), are common for runs at PT conditions close to the decomposition curve (Figure 3.3). Within the limits of analytical errors, three small grunerite grains, annealed at 1250 bars pressure and 612°C for 7 days, show no compositional change. Thus, this PT condition, 1250 bars 612°C, is presumed to be within the stability field of grunerite, but are not sufficent to demonstrate equilibrium. However, the results are comparable with those of Fonarev and his co-workers which clearly show that the upper thermal stability of synthetic grunerite reported by Forbes (1977) is too high.

From the experimental results, the decomposition reaction for the Mg-rich grunerite (R16782) is:

Mg-rich grunerite ⇒ orthopyroxene + quartz +vapor.

The cell parameters of the pyroxene, determined from 13 reflections, are a =

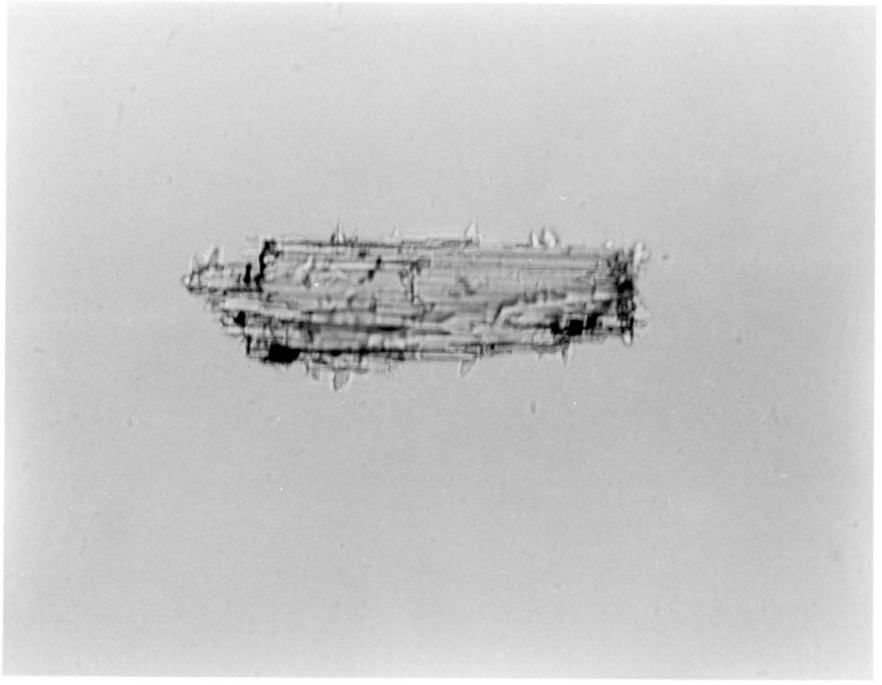

Figure 3.2 Hydrothermally annealed grunerite R7702 with quartz nucleations on the surface. (1.25 kbar, 612°C, 7 days).

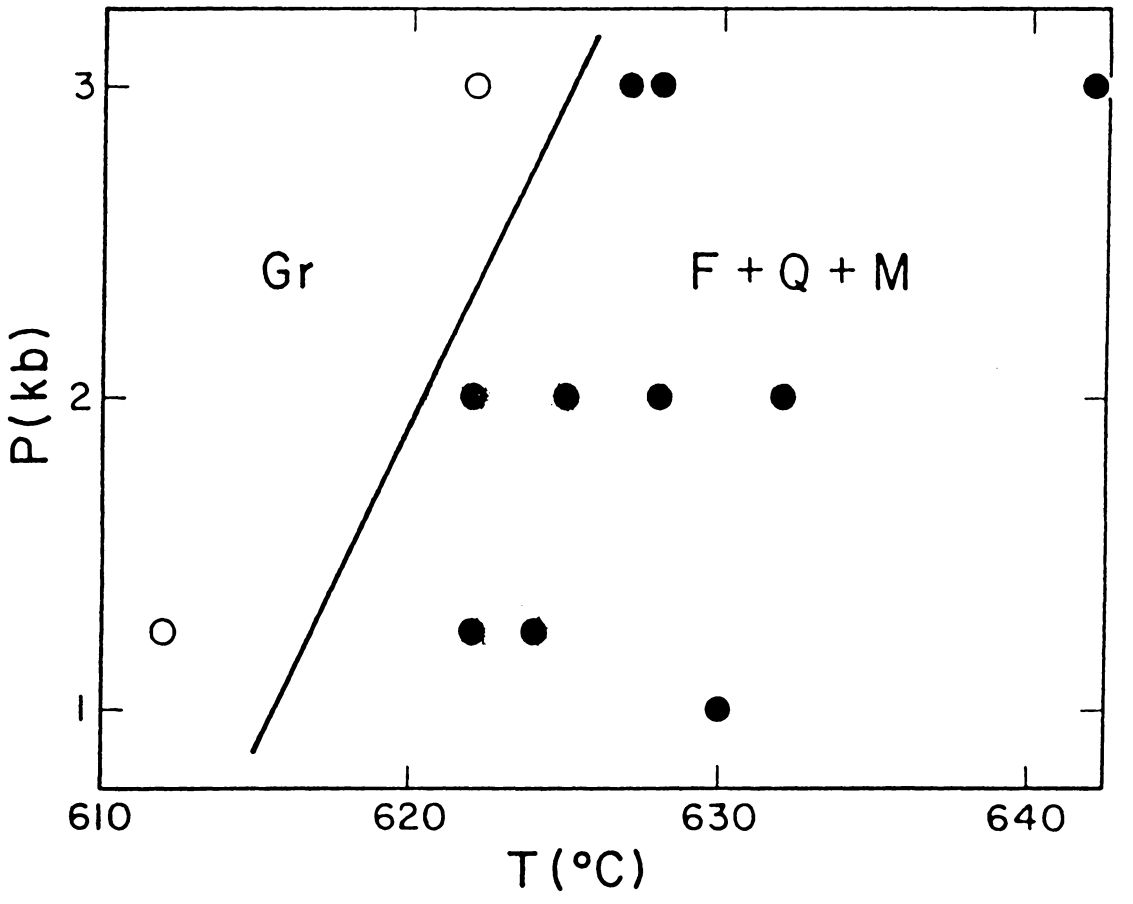

Figure 3.3 P-T diagram for grunerite NMNH #R7702.
(Abbreviations are the same as Table 3.1)

18.36(7)Å, b = 9.08(4)Å, and c = 5.21(1)Å. The Fe/(Fe+Mg) ratio of the orthopyroxene product ranges from 0.711 to 0.744, which is higher than the Fe/(Fe+Mg) ratio of the grunerite R16782 (0.707).

Probe analyses of a large grunerite grain indicate an increase in Fe/(Fe+Mg) ratio near the edge (0.710 -0.712) as compared to the center (0.705-0.707) of the grain. Abundant fluid inclusions were found in grunerite R16782 after it had been hydrothermally treated at high temperatures (Figure 3.4). Fluid inclusions also occur in the pyroxene (Figure 3.5). The fluid inclusions in the grunerite appear to be aligned with the exsolution traces observed by Ross and others (1968, 1969); the fluid inclusions in pyroxene appear to have a random orientation. Because of the temperature limits of our hydrothermal units, the upper thermal stability of grunerite R16782 could not be narrowed down as desired. However, it can be said that the orthopyroxene lower stability brackets at 1, 2, and 3 kbar are 720±5, 725±5 and 730±5°C, respectively, which are comparable with the data reported by Fonarev and Korolkov (1980)(Figure 3.6).

Discussion

Based on the experimental results on specimen R7702, the extrapolated $\log f H_2O$ values for its decomposing reaction at 600°, 700°, and 800°C are 2.27, 5.32 and 7.79, respectively. When these values were plotted against OH stretching frequency at different temperatures (Figure 3.7), the correlation coefficients for 600, 700 and 800°C are -0.75, -0.87, and -0.81, respectively. This, again, supports the hypothesis that the OH bond strength plays an important role in the hydrothermal stability of amphiboles.

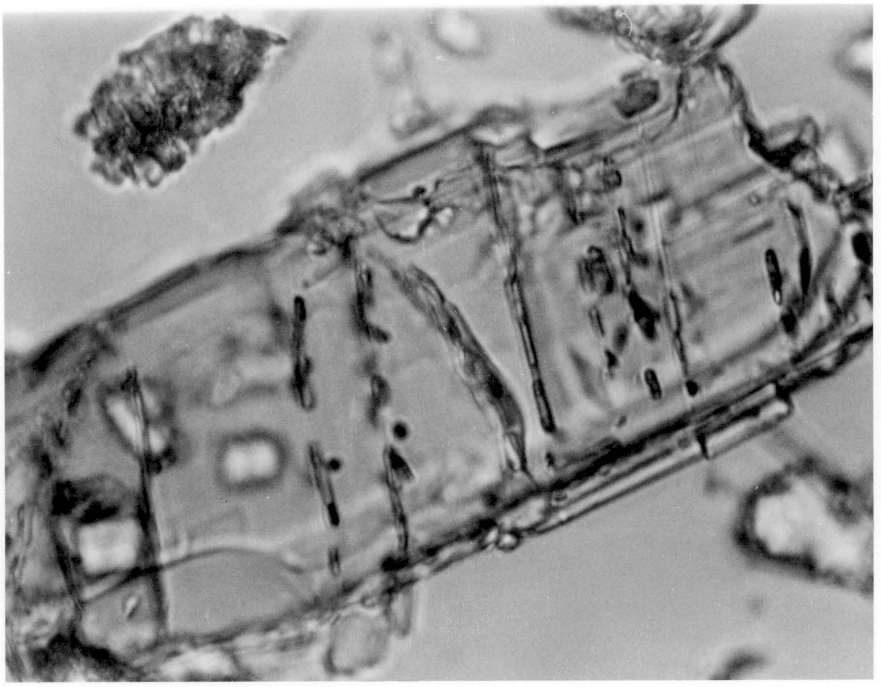

Figure 3.4 Fluid inclusions in hydrothermally annealed grunerite R16782.

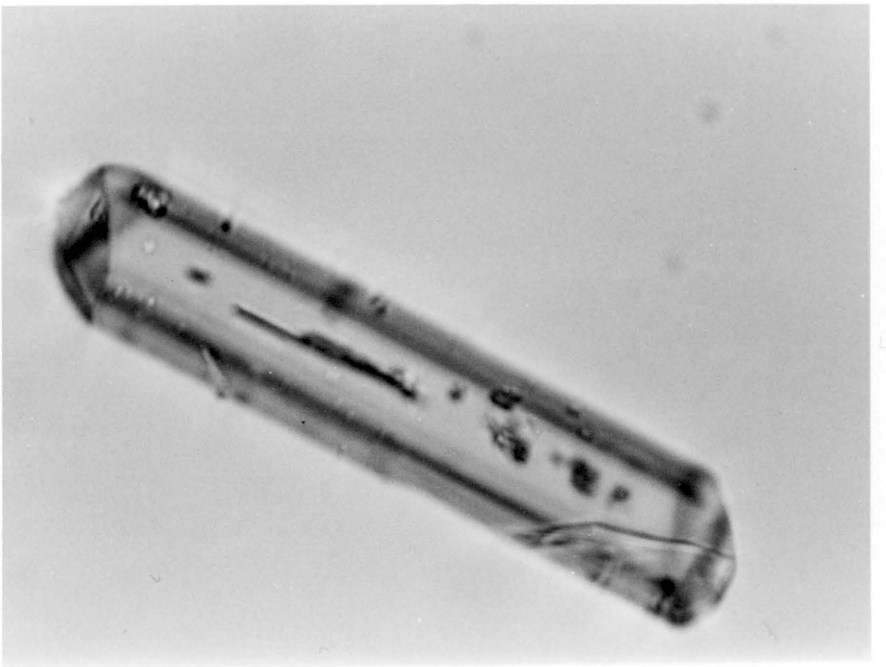

Figure 3.5 Fluid inclusions in orthopyroxene phase in the run product.

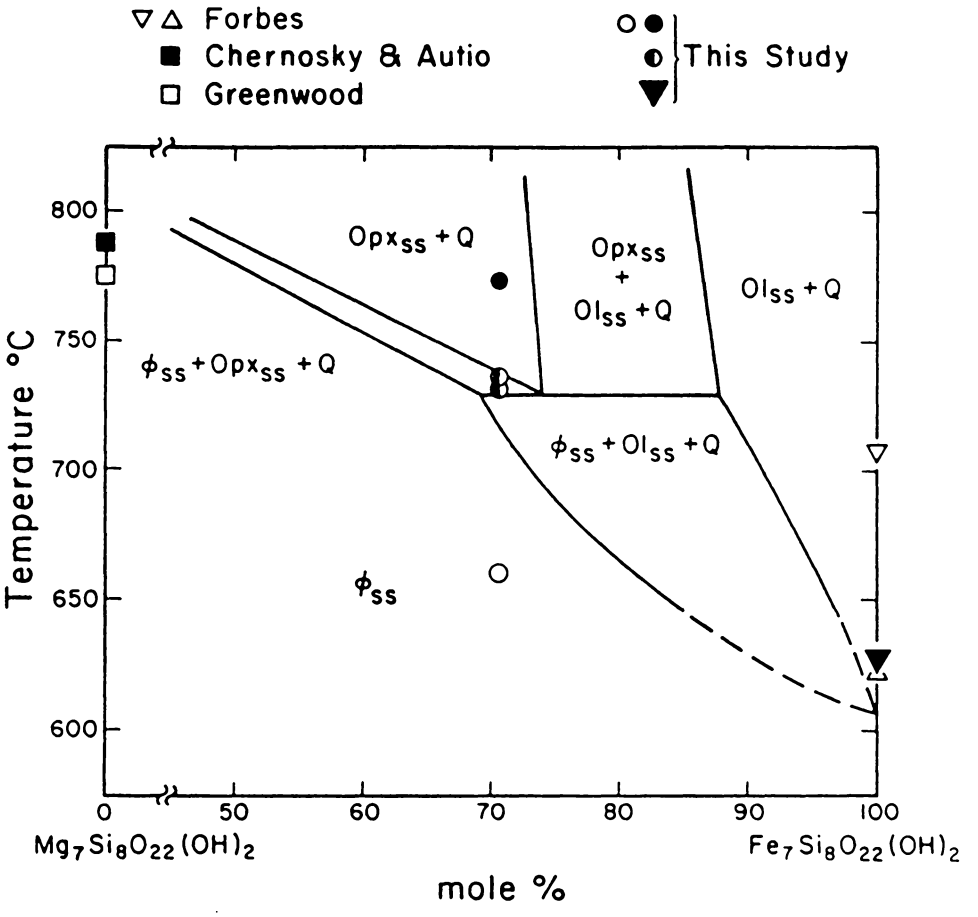

Figure 3.6 T-X sectionon the Mg7-Fe7 join at 2940 bar.

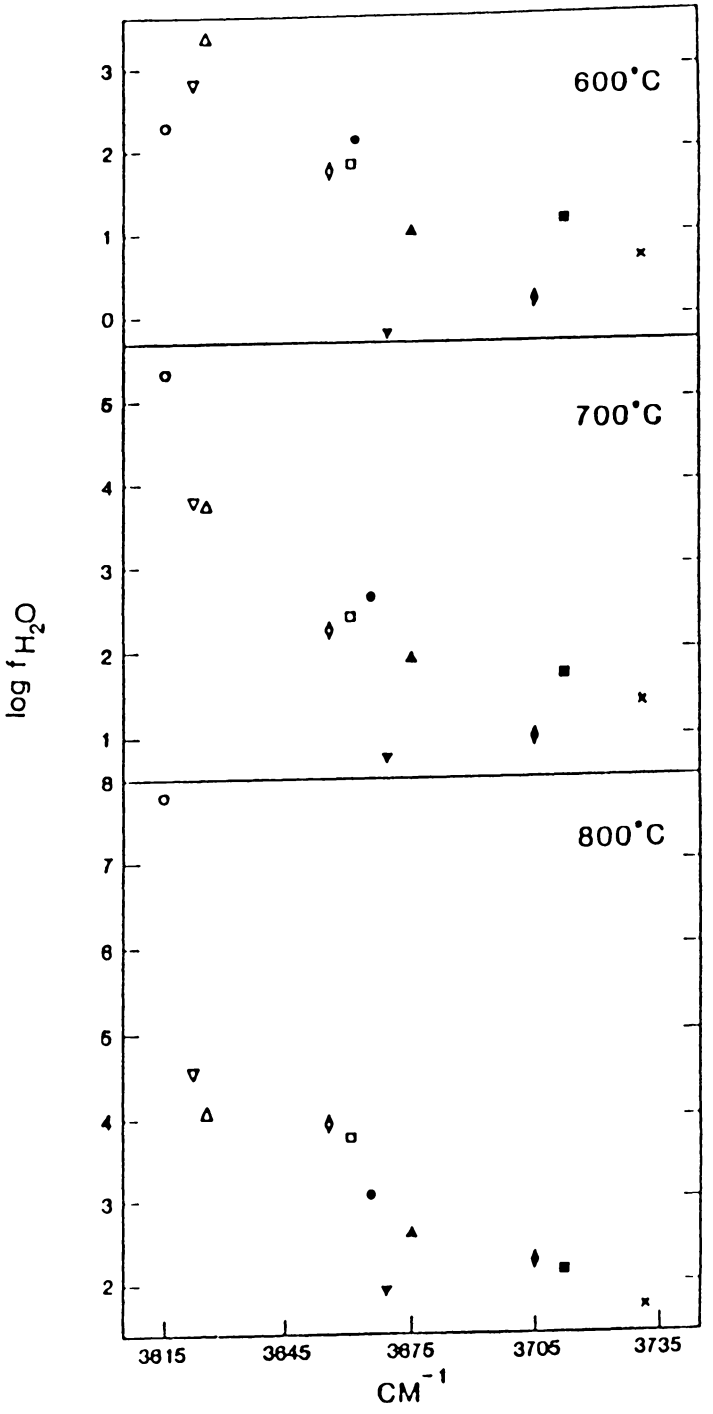

Figure 3.7 LogfH_2O versus OH stretching frequency at different temperatures.
(symbols are the same as in Figure 2.2)

These two different breakdown reactions are controled both structurally and compositionally. The reported compositional range of prograded grunerite-olivine pairs are $X_{Fe} > 0.7$ and $X_{Fe} > 0.85$ (Morey *et al.*, 1972; Gole and Klein, 1981). The reported grunerite-orthopyroxene pairs in metamorphosed iron formations have a $X_{Fe} < 0.8$ for grunerite and a $X_{Fe} < 0.85$ for orthopyroxene (Butler, 1969; Bonnichsen, 1969; Morey *et al*, 1972; Immega and Klein, 1976; Klein, 1978; Vaniman *et al.*, 1980; Gole and Klein, 1981) and Fe is more enriched in the orthopyroxene than in grunerite. Fe-rich orthopyroxene, ferrosilite, was not stable under the experimental conditions.

The Fe/(Fe+Mg) ratio of grunerite R16782 is 0.707. Increase of the Fe/(Fe+Mg) ratios near the edges of the grain suggests migration of cations during hydrothermal treatment. Structural and chemical analyses of a natural metamorphic hornblende annealed over different oxygen fugacities (Phillips *et al.*, 1986) also indicate cation migration, even with only 30 minutes of heating. The high X_{Fe} in orthopyroxene is consistent with the data reported by Fornarev and Korolkov (1980) and also with pairs found in natural environments (e.g., Butler, 1969; Klein, 1978; Gole and Klein, 1981).

CHAPTER 4. FE/MG ORDERING IN CUMMINGTONITE AND GRUNERITE STRUCTURES

Introduction

The crystal structure of grunerite Klein No. 9A has been refined and compared with two other refined structures (Fisher, 1966; Finger, 1969) of amphiboles in the cummingtonite-grunerite series in order to correlate structural changes with Fe substitution for Mg and to delineate the relationships between structure and thermal stability.

Experiments

The grunerite sample No. 9A of Klein (1964) used in this study is from the Wabush iron formation, Labrador, Canada. The chemical formula was simplified from $Na_{0.04}K_{0.04}Ca_{0.03}Fe_{5.35}Mg_{1.55}Si_{7.92}Al_{0.08}O_{22}(OH,F)_2$ (reported by Klein, 1964) to $Fe_{5.45}Mg_{1.55}Si_8O_{22}(OH)_2$ for this refinement.

The crystal selected, 0.08 x 0.17 x 0.23 mm in size, is bounded by (110), $(\bar{1}\bar{1}0)$ and $(1\bar{1}0)$ cleavage planes on three sides. The unit-cell parameters, determined by least-squares refinement of 18 high angle reflections collected on a Picker 4-circle, single crystal diffractometer are given in Table 4.1.

X-ray intensity data were collected automatically, with Nb-filtered Mo radiation (λ = 0.71069 Å), in a constant precision scan mode with 4 minutes maximum time for each reflection and with 0.01 precision. Reflections of the type hkl and $\bar{h}k\bar{l}$ with $2\theta < 75°$ were collected. With the general absorption correction program of Burnham (1966), the integrated intensities were converted to structure factors by applying the correction for Lorentz polarization and absorption (μ = 50.14 cm^{-1}), using a six, eight, six-point

Table 4.1 Crystal data for three cummingtonite-grunerite samples

	cummingtonite Ghose (1961) Fisher (1966)	grunerite Klein 9A This study	grunerite Klein 1 Finger (1969)
a(Å)	9.516(5)	9.548(1)	9.564(1)
b(Å)	18.139(10)	18.319(2)	18.393(2)
c(Å)	5.311(5)	5.333(1)	5.339(1)
β(°)	102.1(1)	101.846(8)	101.892(3)
Volume(Å^3)	896.4	912.9(2)	919.0(2)
Space Group	C2/m	C2/m	C2/m
Chemistry			
Si	7.90	7.92	8.00
Al	0.10	0.08	0.00
Fe	2.50	5.50	6.14
Mg	4.05	1.59	0.77
Mn	0.17	0.08	0.05
Ca	0.35	0.03	0.06
Na	0.00	0.04	0.00
K	0.00	0.04	0.00
Locality	Iron formation Quebec, Canada Canada	Wabush Iron Formation Labrador, Canada	Wabush Iron Formation Labrador,

Estimated standard deviations, σ, given in parentheses.

Gaussian quadrature integration. Only reflections with F(obs) of greater than 3σ were used in the refinement.

Structure Refinement

A least-squares refinement of the grunerite structure in space group C2/m was made using RFINE4 program (Finger and Prince, 1975), the atomic coordinates and temperature factors of grunerite (Finger, 1969) as starting parameters, neutral atom scattering factors (Doyle and Turner, 1968), and anomalous scattering coefficients (Cromer, 1965). As a starting point, a completely disordered structure was assumed. The total chemistry was constrained to agree with the chemical analysis throughout the refinement. The final residual of unit weight for this crystal was 0.055 for the 3751 reflections used in the refinement and 0.095 for all 3987 reflections. The final standard deviation of an observation of unit weight was 1.77, and the final value of the Hamilton (1965) weighted residual was 0.031.

The positional parameters, occupancies, and anisotropic temperature factors were refined simultaneously. The final positional parameters and equivalent isotropic temperature factors of Hamilton (1959) for grunerite 9A are compared with two other Fe-Mg amphiboles and are listed in Table 4.2 according to the Fe/(Fe+Mg) ratio, increasing toward the right. The anisotropic temperature factors of grunerite 9A are presented in Table 4.3. The root-mean-square (rms) amplitude of the principal axes of the thermal ellipsoids and angles between these axes and the direct cell axes, calculated with the program BADTEA (Finger and Prince, 1975), are listed in Table 4.4. Selected interatomic distances and angles and the M(1), M(2), M(3) and

Table 4.2 Positional parameters and temperature factors for three cummingtonite-grunerite samples

Atom	Parameter	Cummingtonite Fisher (1966)	Grunerite Klein 9A This study	Grunerite Klein 1 Finger (1969)
M(3)	B	0.23	0.59(2)	0.56(5)
M(1)	y	0.0872(1)	0.0878(2)	0.08781(8)
	B	0.23	0.55(1)	0.51(3)
M(2)	y	0.1773(1)	0.17905(2)	0.17936(9)
	B	0.27	0.54(1)	0.51(4)
M(4)	y	0.2597(1)	0.25796(2)	0.25741(8)
	B	0.88	0.82(1)	0.92(4)
T(1)	x	0.2874(2)	0.28652(5)	0.2867(2)
	y	0.0842(1)	0.08368(2)	0.0836(1)
	z	0.2746(3)	0.27052(8)	0.2707(3)
	B	0.36(3)	0.46(1)	0.44(3)
T(2)	x	0.2977(2)	0.29854(5)	0.2993(2)
	y	0.1688(1)	0.16734(2)	0.1667(1)
	z	0.7817(3)	0.77751(8)	0.7780(4)
	B	0.43(3)	0.50(1)	0.49(3)
O(1)	x	0.1135(4)	0.1136(1)	0.1120(5)
	y	0.0874(2)	0.08832(7)	0.0882(2)
	z	0.2087(9)	0.2064(2)	0.2044(9)
	B	0.52(6)	0.65(2)	0.67(8)
O(2)	x	0.1232(4)	0.1253(1)	0.1253(4)
	y	0.1721(2)	0.17372(7)	0.1735(2)
	z	0.7193(9)	0.7167(2)	0.7142(8)
	B	0.67(6)	0.71(2)	0.59(7)
O(3)	x	0.1134(7)	0.1146(3)	0.1147(7)
	y	0.0	0.0	0.0
	z	0.7067(13)	0.7057(4)	0.7035(13)
	B	0.81(8)	0.84(3)	1.09(12)
O(4)	x	0.3798(5)	0.3834(1)	0.3839(5)
	y	0.2460(2)	0.24276(7)	0.2416(2)
	z	0.7716(9)	0.7684(2)	0.7689(8)
	B	0.89(6)	0.84(2)	0.58(7)
O(5)	x	0.3514(4)	0.3502(1)	0.3483(5)
	y	0.1310(2)	0.12897(7)	0.1275(2)
	z	0.0659(9)	0.0573(2)	0.0519(8)
	B	0.89(6)	0.93(2)	0.77(7)
O(6)	x	0.3488(5)	0.3486(1)	0.3478(4)
	y	0.1185(2)	0.11825(8)	0.1182(2)
	z	0.5597(9)	0.5524(2)	0.5530(8)
	B	1.01(7)	1.10(2)	0.86(8)
O(7)	x	0.3417(7)	0.3401(2)	0.3376(6)
	y	0.0	0.0	0.0
	z	0.2719(13)	0.2698(4)	0.2700(13)
	B	0.88(5)	1.00(3)	0.74(11)

Estimated standard deviations, σ, given in parentheses.

Table 4.3 Anisotropic temperature factors for grunerite Klein #9A

Atom	β_{11}	β_{22}	β_{33}	β_{12}	β_{13}	β_{23}
M(3)	0.00200(7)	0.00037(2)	0.0051(2)	0.0	0.00056(7)	0.0
M(1)	0.00194(5)	0.00042(1)	0.0045(1)	0.0	0.00105(5)	0.0
M(2)	0.00174(5)	0.00036(1)	0.0050(2)	0.0	0.00090(6)	0.0
M(4)	0.00230(4)	0.00077(1)	0.0065(1)	0.0	0.00179(5)	0.0
T(1)	0.00135(4)	0.00034(1)	0.0043(1)	-0.00006(2)	0.00058(6)	0.00001(3)
T(2)	0.00141(4)	0.00041(1)	0.0043(1)	-0.00012(2)	0.00065(5)	0.00002(3)
O(1)	0.0017(1)	0.00056(3)	0.0055(3)	-0.00005(5)	0.0005(1)	-0.00006(7)
O(2)	0.0019(1)	0.00058(3)	0.0064(3)	-0.00000(5)	0.0007(1)	0.00008(8)
O(3)	0.0025(2)	0.00058(4)	0.0083(5)	0.0	0.0013(3)	0.0
O(4)	0.0027(1)	0.00054(3)	0.0079(3)	-0.00043(5)	0.0008(2)	0.00022(8)
O(5)	0.0021(1)	0.00092(3)	0.0078(3)	0.00002(5)	0.0011(2)	0.00115(8)
O(6)	0.0020(1)	0.00132(4)	0.0075(3)	0.00025(6)	0.0004(2)	-0.00138(9)
O(7)	0.0025(2)	0.00040(4)	0.00149(6)	0.0	0.0014(3)	0.0

Estimated standard deviations, σ, given in parentheses.

Table 4.4 Magnitudes and orientation of priciple axes of thermal ellipsoids in grunerite 9A

Atom, axis	rms displacement Å(σ)	Angles in degrees, with respect to +a(σ)	+b(σ)	+c(σ)
M(3), 1	0.080 (2)	90	0	90
2	0.084 (2)	92 (6)	90	166 (6)
3	0.095 (2)	2 (6)	90	104 (6)
M(1), 1	0.074 (1)	117 (6)	90	15 (6)
2	0.085 (1)	90	180	90
3	0.094 (1)	27 (6)	90	75 (6)
M(2), 1	0.079 (1)	90	0	90
2	0.079 (1)	53 (10)	90	155 (10)
3	0.089 (1)	37 (10)	90	65 (10)
M(4), 1	0.080 (1)	134 (1)	90	32 (1)
2	0.108 (1)	136 (1)	90	122 (1)
3	0.114 (1)	90	0	90
T(1), 1	0.072 (1)	132 (12)	135 (12)	68 (12)
2	0.077 (1)	87 (12)	112 (12)	156 (12)
3	0.080 (1)	42 (12)	127 (12)	82 (12)
T(2), 1	0.072 (1)	139 (6)	118 (5)	52 (7)
2	0.078 (1)	110 (6)	110 (5)	142 (7)
3	0.088 (1)	55 (6)	145 (5)	92 (7)
O(1), 1	0.085 (2)	39 (25)	79 (17)	75 (23)
2	0.089 (2)	53 (25)	90 (17)	115 (23)
3	0.098 (2)	81 (25)	169 (17)	86 (23)
O(2), 1	0.091 (2)	7 (30)	85 (23)	106 (23)
2	0.093 (2)	96 (30)	72 (23)	155 (23)
3	0.100 (2)	94 (30)	19 (23)	71 (23)
O(3), 1	0.099 (4)	90	0	90
2	0.100 (4)	32 (15)	90	133 (15)
3	0.110 (4)	59 (15)	90	43 (15)
O(4), 1	0.079 (3)	124 (3)	145 (3)	74 (4)
2	0.104 (2)	105 (6)	91 (5)	154 (5)
3	0.122 (2)	142 (4)	55 (3)	69 (6)
O(5), 1	0.082 (3)	113 (8)	121 (2)	35 (3)
2	0.097 (3)	157 (8)	80 (5)	99 (7)
3	0.139 (2)	93 (3)	33 (2)	57 (2)
O(6), 1	0.085 (3)	112 (18)	64 (2)	29 (10)
2	0.092 (3)	154 (16)	89 (9)	104 (17)
3	0.162 (2)	102 (2)	153 (1)	65 (1)
O(7), 1	0.083 (4)	90	0	90
2	0.104 (4)	176 (4)	90	82 (4)
3	0.143 (4)	94 (4)	90	8 (4)

Estimated standard deviations, σ, given in parentheses.

M(4) site occupancies are shown in Tables 4.5, 4.6, and 4.7.

Discussion

Before comparing the three structures, the reader is reminded of the following: Ghose and Hellner (1959) and Ghose (1961) examined the cummingtonite structure and determined the Fe/Mg distribution by adjusting the site occupancy to obtain uniform isotropic temperature factors for all four cation sites. Fisher (1966) refined the same structure by the least-squares method and obtained different results. Mössbauer spectrum of this amphibole (Hafner and Ghose, 1971) indicates a $Fe_{M(4)}/Fe_{M(1,2,3)}$ ratio of 0.73/0.20, which is different from the values of 0.75/0.26 (Ghose, 1961) and of 0.87/0.12 (Fisher, 1966). The lattice constants reported by Ghose (1961) differ from those reported by Viswanathan and Ghose (1965) for the same composition. The inconsistency in their results may reflect errors dependent upon the bond lengths, bond angles, and occupancies for this cummingtonite are larger than would be expected. The bond lengths, bond angles, and their associated errors used in the present study are taken from Hawthorne (1983). They were recalculated by taking the positional parameters from Fisher (1966) and the cell parameters from Viswanathan and Ghose (1965). Mitchell *et al.* (1971) applied the same justification before they compared the structure with that of actinolite. The polyhedral site occupancy data were taken from Fisher (1966).

Table 4.5 Interatomic distances (Å) in tetrahedral chains for three cummingtonite-grunerite samples

Atom	Cummingtonite Ghose (1961)	Grunerite Klein 9A This study	Grunerite Klein 1 Finger (1969)
T(1)-O(1)	1.619(7)	1.618(1)	1.637(4)
T(1)-O(5)	1.614(7)	1.623(1)	1.627(5)
T(1)-O(6)	1.628(7)	1.627(1)	1.630(4)
T(1)-O(7)	1.613(7)	1.616(1)	1.613(2)
Average	1.619	1.621	1.627
T(2)-O(2)	1.625(7)	1.623(1)	1.633(4)
T(2)-O(4)	1.609(7)	1.607(1)	1.604(4)
T(2)-O(5)	1.639(7)	1.631(1)	1.611(5)
T(2)-O(6)	1.643(7)	1.648(1)	1.638(5)
Average	1.629	1.628	1.622
	O-O distances (Å)		
T(1) tetrahedra			
O(1)-O(5)	2.654(6)	2.651(2)	2.656(6)
O(1)-O(6)	2.656(6)	2.654(2)	2.669(6)
O(1)-O(7)	2.652(7)	2.666(2)	2.664(6)
O(5)-O(6)	2.638(8)	2.651(2)	2.682(6)
O(5)-O(7)	2.626(5)	2.631(2)	2.629(5)
O(6)-O(7)	2.630(6)	2.630(2)	2.638(6)
Average	2.643	2.647	2.656
T(2) tetrahedra			
O(2)-O(4)	2.748(6)	2.733(2)	2.733(6)
O(2)-O(5)	2.642(6)	2.642(2)	2.633(6)
O(2)-O(6)	2.653(7)	2.668(2)	2.657(6)
O(4)-O(5)	2.654(6)	2.649(2)	2.649(6)
O(4)-O(6)	2.562(6)	2.546(2)	2.536(6)
O(5)-O(6)	2.693(6)	2.697(2)	2.668(6)
Average	2.659	2.656	2.646
	T-T distances(Å)		
T(1)-T(2)	3.083(4)	3.089(1)	3.090(3)
T(1)-T(2)	3.054(4)	3.066(1)	3.066(3)
T(1)-T(1)	3.055(3)	3.066(1)	3.075(4)

Estimated standard deviations, σ, given in parentheses.

Table 4.6 Interatomic angles (°) in the tetrahedral chains for three cummingtonite-grunerite samples

Atoms	Cummingtonite Fisher (1966)	Grunerite Klein 9A This study	Grunerite Klein 1 Finger(1969)
O(1)-T(1)-O(5)	110.4(2)	109.74(7)	108.9(2)
O(1)-T(1)-O(6)	109.7(3)	109.74(7)	109.6(2)
O(1)-T(1)-O(7)	110.3(3)	111.03(8)	110.1(3)
O(5)-T(1)-O(6)	108.9(3)	109.29(7)	110.9(2)
O(5)-T(1)-O(7)	108.9(3)	108.60(9)	108.5(3)
O(6)-T(1)-O(7)	108.7(3)	108.41(9)	108.9(3)
Average	109.5	109.47	109.5
O(2)-T(2)-O(4)	116.3(2)	115.55(7)	115.2(2)
O(2)-T(2)-O(5)	108.1(2)	108.54(7)	108.5(2)
O(2)-T(2)-O(6)	108.5(2)	109.28(7)	108.7(2)
O(4)-T(2)-O(5)	109.6(2)	109.78(8)	110.9(2)
O(4)-T(2)-O(6)	103.9(3)	102.93(7)	103.0(2)
O(5)-T(2)-O(6)	110.3(2)	110.65(7)	110.4(2)
Average	109.5	109.45	109.5
T(1)-O(5)-T(2)	139.7(3)	140.8(1)	142.4(3)
T(1)-O(6)-T(2)	141.0(3)	141.3(1)	142.1(3)
T(1)-O(7)-T(1)	142.4(5)	143.1(1)	144.8(4)
O(5)-O(6)-O(5)	170.2(2)	171.6(1)	172.7(3

Estimated standard deviations, σ, given in parentheses.

Table 4.7 Interatomic distance (Å) in the octahedral strip for three cummingtonite-grunerite samples

Atoms	Cummingtonite Fisher (1966) Site occupancy	Cummingtonite Fisher (1966) distance	Grunerite Klein #9A This study Site occupancy	Grunerite Klein #9A This study distance	Grunerite Klein #1 Finger (1969) Site occupancy	Grunerite Klein #1 Finger (1969) distance
M(1)-O(1)		2.064(7)		2.080(1)		2.082(5)
M(1)-O(2)	0.16 Fe	2.128(7)	0.753(5) Fe	2.162(1)	0.848(8) Fe	2.160(4)
M(1)-O(3)	0.84 Mg	2.091(7)	0.247 Mg	2.120(1)	0.152 Mg	2.122(4)
mean for 6		2.094		2.121		2.121
M(2)-O(1)		2.134(7)		2.159(1)		2.161(5)
M(2)-O(2)	0.05 Fe	2.083(7)	0.586(5) Fe	2.113(1)	0.773(7) Fe	2.128(4)
M(2)-O(4)	0.95 Mg	2.033(7)	0.414 Mg	2.062(1)	0.227 Mg	2.075(4)
mean for 6		2.083		2.111		2.121
M(3)-O(1)	0.16 Fe	2.099(7)	0.795(7) Fe	2.125(1)	0.888(12) Fe	2.118(5)
M(3)-O(3)	0.84 Mg	2.073(7)	0.205 Mg	2.089(2)	0.112 Mg	2.103(6)
mean for 6		2.083		2.114		2.113
M(4)-O(2)		2.164(7)		2.140(1)		2.135(5)
M(4)-O(4)		2.023(7)		1.986(1)		1.988(4)
M(4)-O(6)	0.87 Fe	2.691(7)	0.983(8) Fe	2.734(1)	0.985(8) Fe	2.757(5)
M(4)-O(5)	0.13 Mg	3.143(7)	0.017 Mg	3.244(1)	0.015 Mg	3.298(5)
mean for 6		2.293		2.287		2.293
mean for 8		2.505		2.526		2.545
M(1)-M(1)		3.163(3)		3.217(1)		3.230
M(1)-M(2)		3.118(4)		3.147(1)		3.156
M(1)-M(3)		3.091(4)		3.114(1)		3.120
M(1)-M(4)		3.129(3)		3.117(1)		3.119
M(2)-M(3)		3.216(3)		3.281(1)		3.299
M(2)-M(4)		3.047(4)		3.033(1)		3.031

Estimated standard deviations, σ, given in parentheses.

The T(1) and T(2) Tetrahedra

Negligible thermal expansion of the tetrahedra in amphiboles has been reported in several high temperature crystal structural refinements (Prewitt *et al.*, 1970; Sueno *et al.*, 1972, 1973; Cameron *et al.*, 1973a, b; Cameron and Papike, 1979). Changes in the T-O and O-O distances are insignificantly small.

The data for the three Fe-Mg amphibole structures considered in this study show that (1) the mean T(1)-O distance increases with increasing Fe content, (2) the mean T(2)-O distance decreases, and (3) the mean O-O distance increases with Fe content in the T(1) site and decreases in the T(2) site. This suggests that the tetrahedra respond quite differently to heating than to Fe $\rightarrow$ Mg substitution. However , the T-T distances and T-O-T angles increase in both cases.

With large increases in the M-O(1) distances, lengthening of the T(1)-O(1) distance may result primarily as a consequence of the enlarging of the T-O-T angle upon substitution. The observed T(1)–O(7) bond length and the observed T–O(7)–T angles, which were plotted together with the optimized T–O(br)–T angle and T–O bond length derived for $H_6Si_2O_7$ from Gaussian 82 calculations (Gibbs, 1986 personal communication), are shown in Figure 4.1. The observed values are within the estimated errors of the curve.

Within the limits of experimental errors, the T(2)-O(2) bond seems to be the only one showing slight increase with Fe substitution. This may reflect the increase of cation repulsion by shortening of the M(4)-O(2) and M(4)-O(4) distances and the virtually 'clamped' T(2)-O(4) distance. The slightly larger T(2) tetrahedron, as in cummingtonite and grunerite 9A, is considered tohave resulted from the higher average oxygen coordination of the T(2)

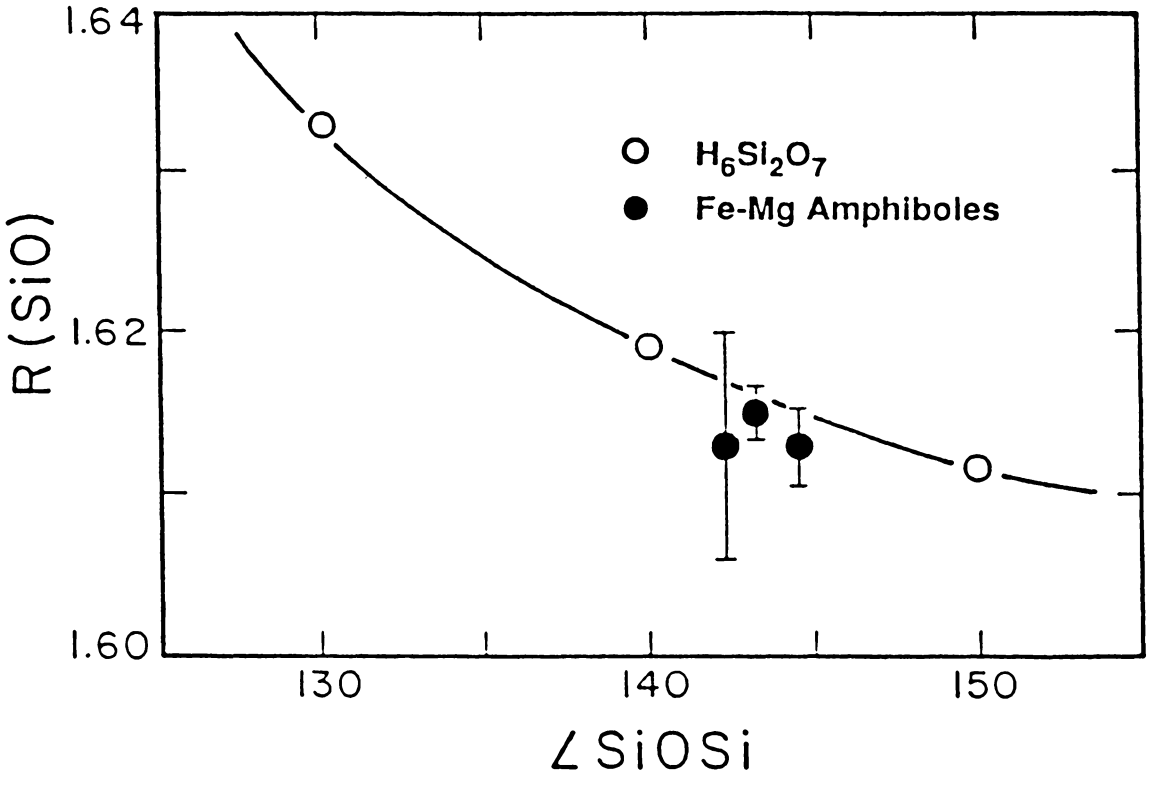

Figure 4.1 R(SiO) versus ∠SiOSi plot.

tetrahedron as compared to that of the T(1) tetrahedron (Gibbs, 1969). For grunerite No.1, the long M(4)-O(5) distance may reflect a lower average oxygen coordination number of the T(2); it is, however, still higher than that of the T(1). The highly underbonded nature of the O(4), reported by Cameron and Gibbs (1973), may serve to explain why the T(2)–O(4) bond length is the shortest tetrahedral bond.

All of the average O-T-O angles are very close to those of the ideal tetrahedron. Except for the O(1)-T(1)-O(7) angle of grunerite No. 1, all of the O(nbr)-T-O(br) angles in the T(1) tetrahedron are larger than the O(br)-T-O(br) angles as discussed by McDonald and Cruickshank (1967). As expected, the O(2)–T(2)–O(4) angle is of the O(nbr)-T-O(nbr) type and is the largest of all O–T–O angles (McDonald and Cruickshank, 1967). The significantly small O(4)–T(2)–O(6) angle exists because the O(4)–O(6) edge is shared between the T(2) tetrahedron and the M(4)-polyhedron. The fact that the M(4)–O(2) and M(4)–O(4) bond lengths are significantly shorter than M(4)–O(5) and M(4)-O(6) bond lengths indicates that the cations occupying the M(4) site are shifted away from the O(5)–O(6) edge shared with T(1) tetrahedron. Thus the cation repulsion is reduced and the O(5)–O(6) distance is no longer the shortest as observed in tremolite and fluor-tremolite (Cameron and Gibbs, 1973).

Enlarging of the T(1) , shrinking of the T(2) tetrahedron, and lengthening of the M(4)-O(5) and M(4)-O(6) distances with increasing Fe-content suggest that when a larger Fe cation enters the structure, it increases the size of the octahedra, squeezes the M(4) group toward the T(2) tetrahedron, compresses the T(2) tetrahedron, and pulls the T(1) tetrahedron open. This indicates that with more Fe present in the structure the double chain linked together by T(1) and T(2) must be under high stress. The angles between the plane defined by

O(4)O(5)O(6) and a^* and between the plane defined by O(7)O(5)O(6) and a^* were calculated by using the MATOP program (Boisen and Gibbs, 1985); they are listed in Table 4.8. The angle between the plane O(4)O(5)O(6) and a^* is related to the bending of the basal plane of the T(2) tetrahedron from the bc–plane. The angle between the plane O(7)O(5)O(6) and a^* is related to the bending of the basal plane of the T(1) tetrahedron from the bc–plane. Clearly, both the T(1) and T(2) tetrahedra are at an angle to the bc–plane and the bending angles increase with increasing Fe content.

Warping of the tetrahedral layer can be seen from the projection of the grunerite No. 1 structure on (001), as prepared with the program ORTEP; this is shown in Figure 4.2. The increase in the T(1)–T(1) distance with increasing Fe-content and the increase in the T(1)–O(7)–T(1) angle suggest that the chain separation increases when Fe occupies the cation sites. The fact that the T(1)–T(1) distance in fluor-tremolite is significantly shorter than that in hydroxyl tremolite was also recorded by Cameron and Gibbs (1973).

The Octahedral Layer

Nonsilicate polyhedra show marked increases in both individual and mean bond lengths that vary linearly with temperature (Prewitt *et al.*, 1970; Sueno *et al.*, 1972, 1973; Cameron *et al.*, 1973a, 1973b; Cameron and Papike, 1979). The mean M-O distances in the three Fe-Mg amphiboles (See Table 4.7) included in this study increase with increasing Fe content. Fe $\rightarrow$ Mg substitution and heating seem to increase the M(4)-O(5) distance significantly. However, the shortening of the M(4)-O(2) distances, and the M(1)-M(4) and the M(2)-M(4) distances with more Fe in the structure is the opposite of

Table 4.8 Tetrahedral chain bending angles

Mineral	a^*^O(4)O(5)O(6)	a^*^O(7)O(5)O(6)	Reference
Grunerite Klein #1	8.69	2.47	Finger, 1969
Grunerite Klein #9A	8.68	2.22	This study
Cummingtonite	7.15	2.04	Fisher, 1966
Mn-Cummingtonite	5.96	1.53	Papike *et al.*, 1969
Cummingtonite(270°C)	6.08	1.51	Sueno *et al.*, 1972
Actinolite	5.75	2.33	Mitchell *et al.*, 1971
Tremolite	4.90	1.68	Hawthorne & Grundy, 1976
Pargasite	5.51	2.53	Bocchio *et al.*, 1978
K-Pargasite	5.16	2.32	Robinson *et al.*, 1970
F-Tremolite	4.65	1.30	Cameron & Gibbs, 1973
K-Richterite	4.65	2.37	Papike *et al.*, 1969
F-Richterite	3.43	1.64	Cameron & Gibbs, 1971
F-Richterite	3.51	1.88	Cameron & Gibbs, 1971
Tremolite	5.04	2.00	Papike *et al.*, 1969
Tremolite(400°C)	5.41	2.10	Sueno *et al.*, 1973
Tremolite(700°C)	5.90	2.01	Sueno *et al.*, 1973

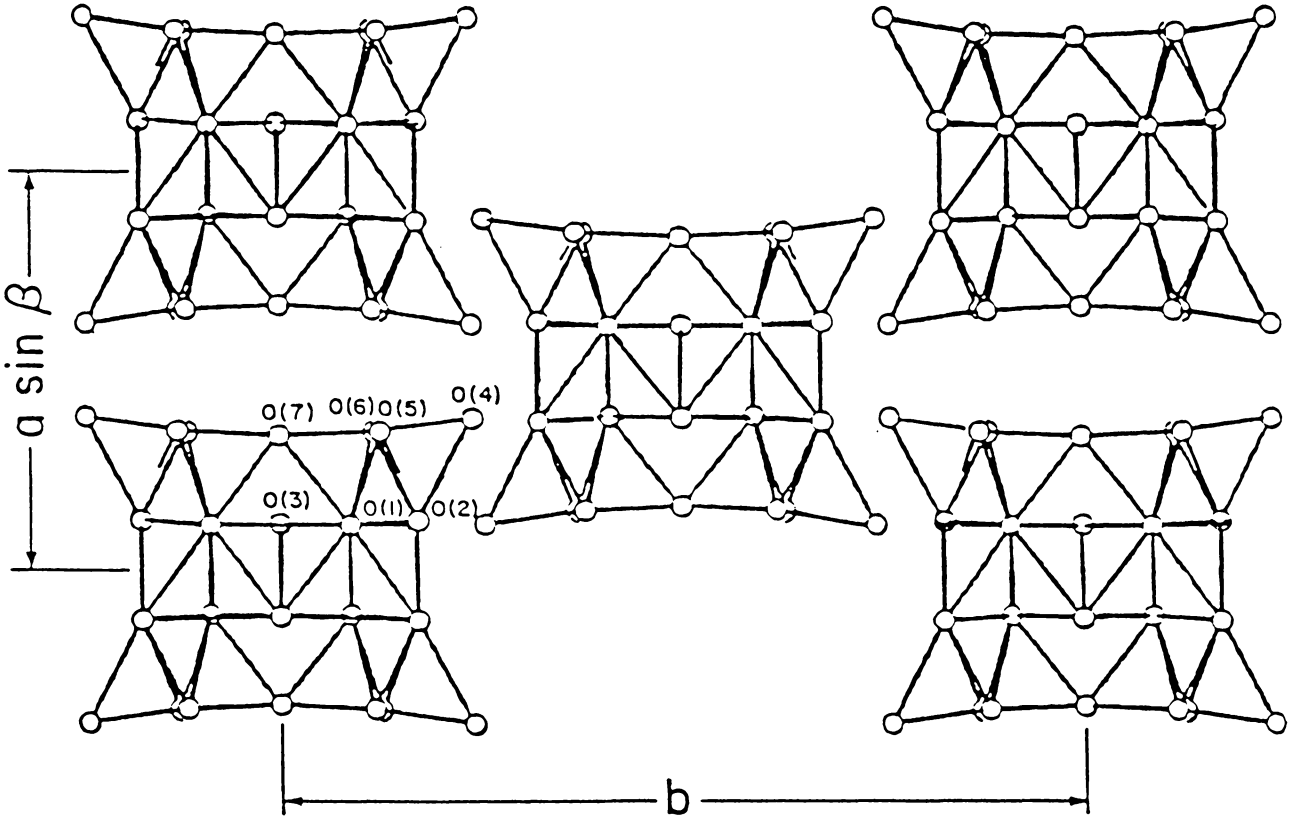

Figure 4.2 Projection of Klein No. 1 grunerite structure on (001).
(prepared using ORTEP)

that obtained from high temperature refinements. This again, reflects the principle that temperature and chemical composition may affect the structure differently.

The octahedral site occupancy determined for grunerite 9A is in general agreement with that found in previous studies (Fisher, 1966; Papike *et al.*, 1969; Finger, 1969). The Fe occupancies of all four cation sites were plotted against the total Fe mole percent (Figure 4.3). The Fe occupancy of the M(3) site of the two grunerite structures is equal to the value of a disordered structure. The M(3) site occupancy of the cummingtonite is ambiguous. The M(1) site is slightly depleted in Fe; the M(2) site is strongly enriched in Mg; the M(4) site is greatly enriched in Fe. The Fe occupancies of the three M(2) sites fall on a straight line ($R > 0.99$) that intercepts the horizontal axis at about 36 mole percent Fe, which is slightly higher than the reported compositional limit of 30 mole percent Fe for natural cummingtonite–grunerite samples (Deer*et al.*, 1962). However, this 36 percent may represent the compositional limit of relatively Al-free monoclinic Fe-Mg amphiboles, which is what these three samples are. Al substitution for Si has been reported for many high-Mg, low-Ca cummingtonites.

Three of the observed mean M-O bond lengths are plotted against the site occupancy (Figure 4.4). The three M(2) sites again fall on a straight line ($R > 0.99$) and give a bond length of 2.08 Å at zero Fe occupancy. This may reflect the minimum average M(2)–O distance that the structure can have and still maintain monoclinic symmetry. The average M(2)–O distance of orthorhombic anthophyllite (Finger, 1968) is 2.076 Å, which is less than 2.08 Å. For the M(3) and M(1) site, the shortest distance of 2.076 Å ($R > 0.99$) and 2.088 Å ($R > 0.9838$), respectively, were inferred from the data. The

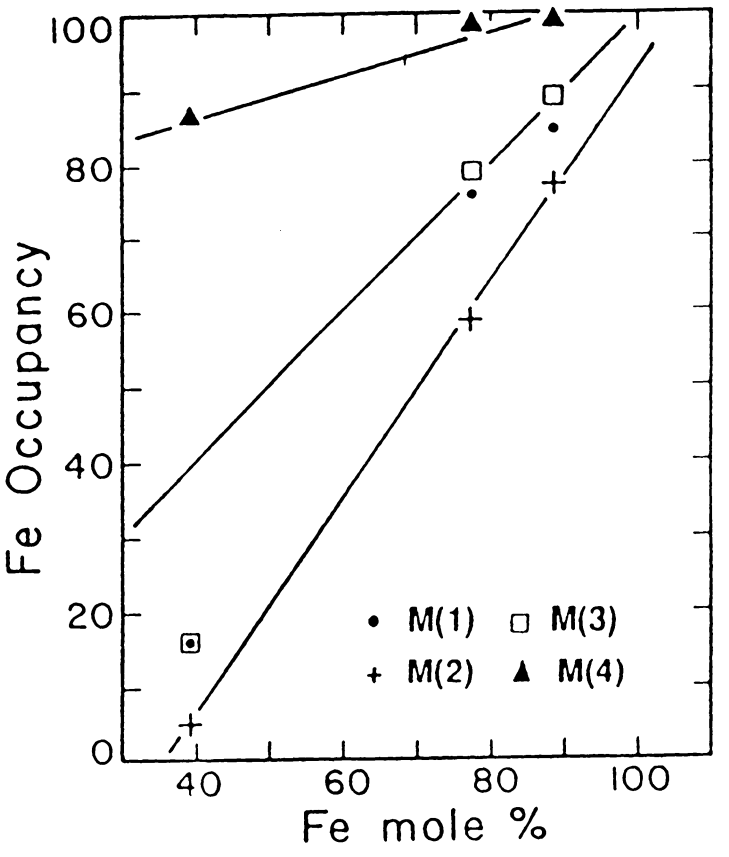

Figure 4.3 Fe occupancy plotted against total mole percent Fe .

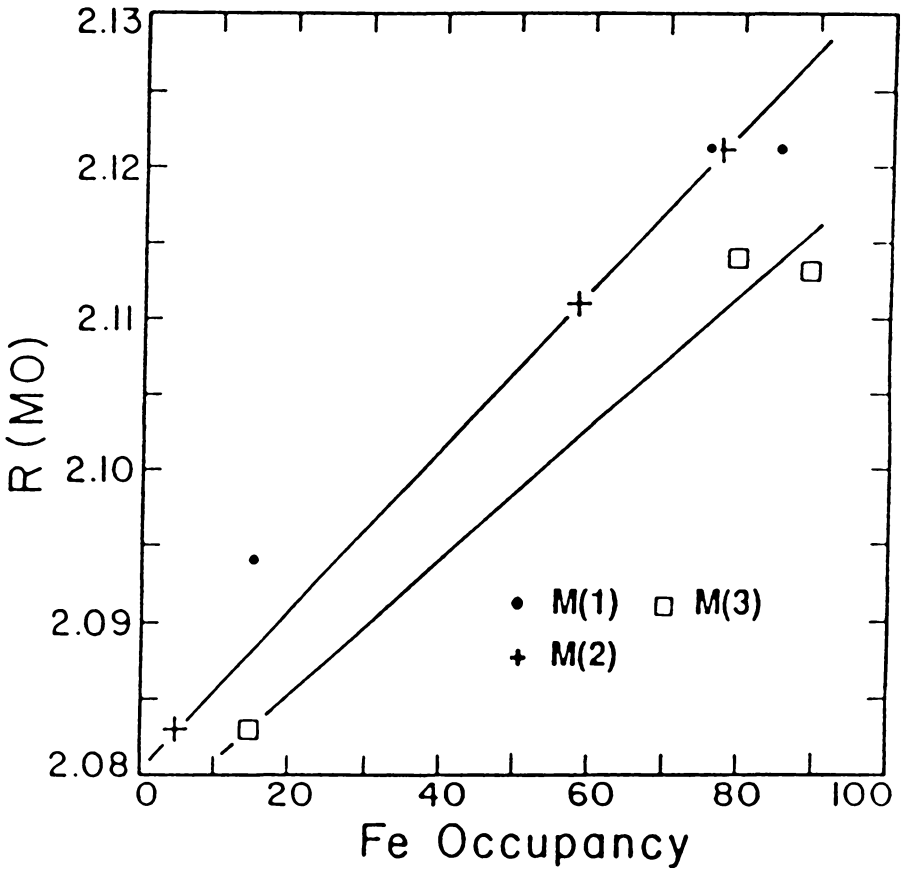

Figure 4.4 Average MO distance plotted against Fe occupancy.

observed average M(3)–O bond length of anthophyllite is 2.070 Å, which is shorter than 2.076 Å. The observed average M(1)–O bond length for anthophyllite is 2.084 Å, which is shorter than 2.088 Å.

The Hydrogen Position

The hydrogen position has also been refined after the structure was converged. The positional parameter and temperature factor of tremolite (Hawthrone and Grundy, 1976) were used as starting values. The positional parameters obtained for this hydrogen atom are x = 0.183(4), z = 0.730(4). The O(3)-H distance, 0.67Å, is short as compared to data reported by Papike *et al.*, (1969) and Hawthorne and Grundy (1976). This OH bond is at an angle of 89.6° (O(3)-O(3)'-H) to the octahedral layer. In addition, large errors and a nonpositive definite temperature factor were obtained. Because of the difficulties in determining the position of H with *x*-ray data, little significance should be attached to the bond lengths and angles involving the atom.

Summary

Klein (1964), Viswanathan and Ghose (1965), and Klein and Waldbaum (1967) reported that the lattice parameters of the cummingtonite-grunerite series vary linearly with composition. All of their results show that the *b* cell edge increases at a much greater rate than *a* and *c*. In fact, the *c* cell dimension changes insignificantly. The substitution of Fe for Mg into the cummingtonite-grunerite structure not only enlarges the octahedral layer but also affects the T(1) and T(2) sites and thus increases strain on the octahedral

and tetrahedral linkage.

High temperature refinements of amphiboles provide further information on the change of structure upon heating. The high thermal expansion of the octahedral layer along with almost no effect on the tetrahedral layer upon heating substantially increases the strain on the structure. This may explain why the Fe-rich end member will decompose at a lower temperature than its Mg-analogue, the structure of which can tolerate the building up of strain to a higher temperature.

CHAPTER 5. CONCLUSIONS

Crystal structure control of the decomposition reactions of Fe-amphiboles is clearly demonstrated by the equilibrium involving cummingtonite-grunerite and Fe-pyroxene (orthopyroxene) and their natural assemblages. Among many of the investigated crystal structural parameters, the T(1)O(7)T(1) angle, the chain separation (T(1)-T(1) distance) and the tetrahedral chain bending angles are thought to be important so far as controlling the stability of the structure and hence the decomposition temperature. High resolution nuclear magnetic resonance studies of minerals are needed to unravel whether or not the physical and chemical behaviors of an atom are same in different neighboring electron configurations; there may be other important factors, such as force constant and local bonding status, at the fine atomic or electronic levels.

Experimental results of this study indicate that the upper thermal stability of the grunerite end-member should be lowered by 50°C. However, the temperature difference is still not as great as other Fe-Mg amphibole pairs (Figure 5.1). Perhaps this is because grunerite-anthophyllite is the only Fe-Mg amphibole pair that belongs to two different crystallographic systems.

The significant correlation between the hydroxyl stretching frequency and the water fugacity data observed in this investigation clearly demonstrates that the thermal stability of amphiboles is affected by the localized force field around the hydrogen. The differences in OH stretching frequencies, cation ordering, and structures observed between natural and synthetic samples suggest that the application of experimental studies to the natural systems should be used only with caution.

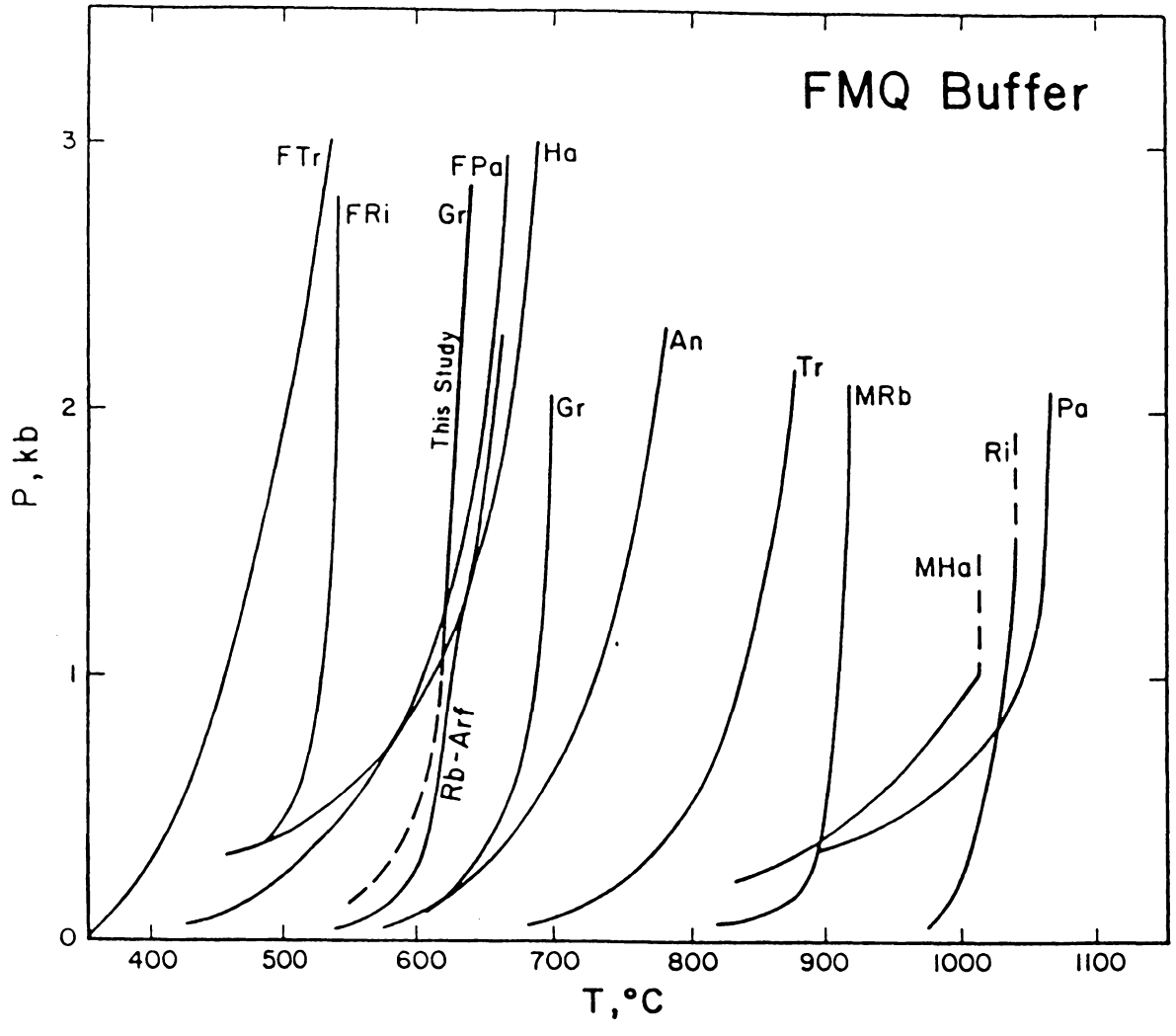

Figure 5.1 Upper thermal stability of several Mg-Fe amphibole pairs.
(Abbreviations are the same as in Figure 1.4)

Strens (1963) concluded that iron (Fe^{+3}) content should raise the decomposition temperature of epidote under oxidizing conditions. Holdaway (1972) confirmed that Fe^{+3} increases the break-down temperature of epidote minerals. Langer and Raith (1974) observed that the OH stretching frequency increases with the Fe^{+3} content in epidotes (Figure 5.2). Along the epidote $\Leftrightarrow$ garnet + anorthite + cordierite + magnetite boundary, the equilibrium temperature increases from 650 to 690°C, whereas the $Fe^{+3}/(Fe^{+3}+Al)$ ratio (p ratio) increases from 0.24 to 0.99 (Holdaway, 1972). The hydroxyl stretching frequency of epidote increases from 3338 cm^{-1} for p = 0.29 to 3365 cm^{-1} for p = 0.89 (Langer and Raith, 1974, See Figure 5.2). Along the epidote $\Leftrightarrow$ garnet + anorthite + quartz + hematite boundary, the decomposition temperature of epidote mineral still increases with increasing p ratio (Figure 5.3). There appears to be a monotonic increase of decomposition temperature with increasing p ratio regardless of what phases are involved in the reactions.

Stability studies of micas have shown that at a given pressure the dioctahedral layer silicates dehydroxylate at lower temperatures than the trioctahedral ones do. Decomposition temperatures of 1060°C for phlogopite and 650°C for muscovite at one kilobar have been reported by Kiefer (1949), Yoder and Eugster (1954, 1955) and DeVries and Roy (1958). The highest hydroxyl stretching frequency (MgMgMg-OH) in phlogopite is 3712 cm^{-1} (Vedder and Wilkins, 1969), whereas that for muscovite is only a broad peak at 3628 cm^{-1} (Vedder and McDonald, 1963) (Figure 5.4).

High hydroxyl stretching frequencies associated with high thermal stabilities of minerals suggests that the OH bond strength is very likely important so far as the thermal stability of all hydroxyl minerals.

The hydroxyl stretching frequencies of different clinoamphiboles were also

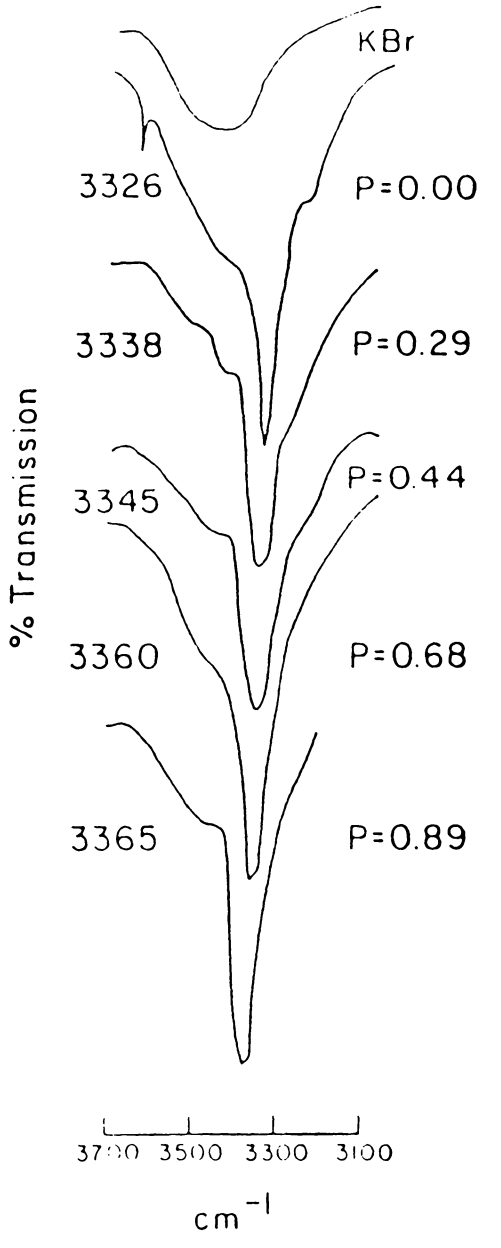

Figure 5.2 Hydroxyl stretching frequencies of epidote (modified after Langer and Raith, 1974).

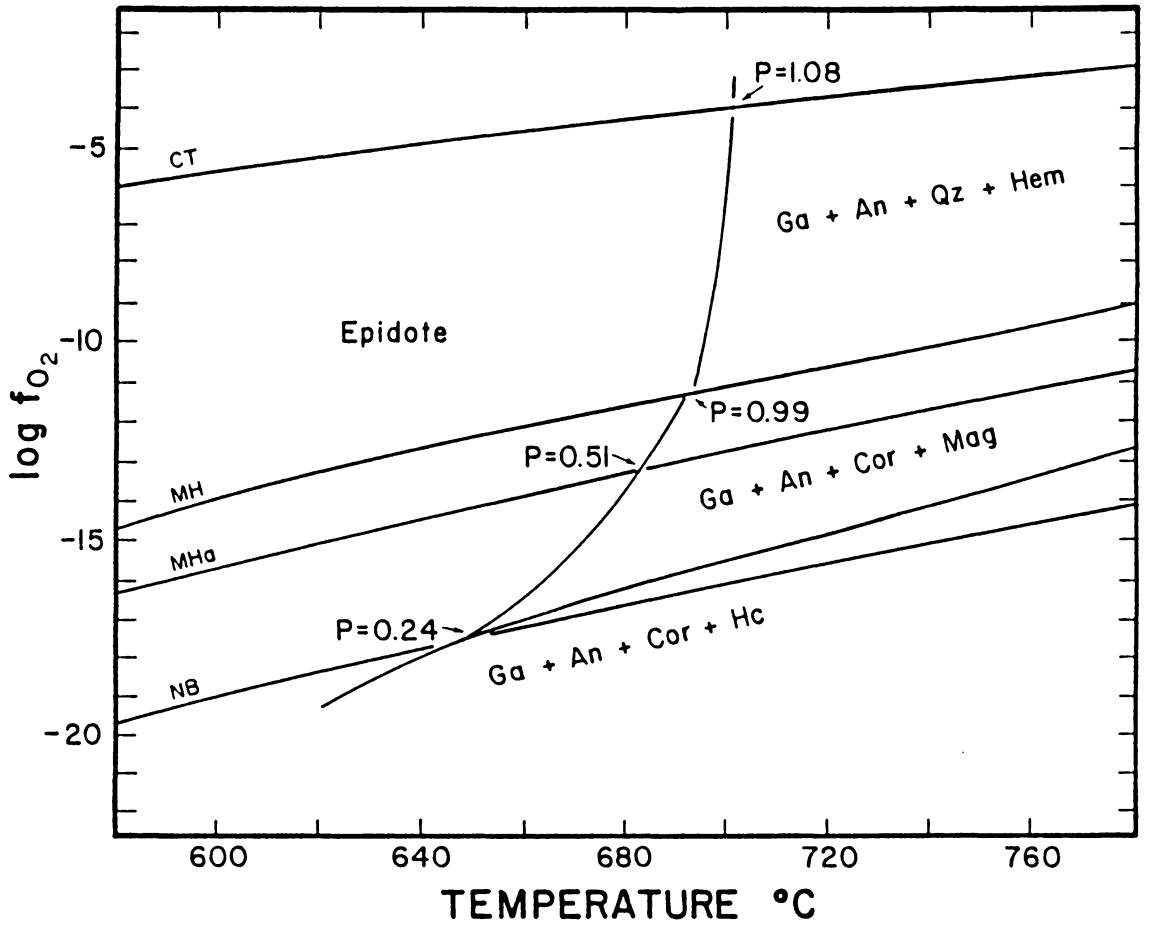

Figure 5.3 fO_2–T for epidote bulk composition, where P = $Fe^{+3}/(Fe^{+3} + Al)$ (modified after Holdaway, 1972).

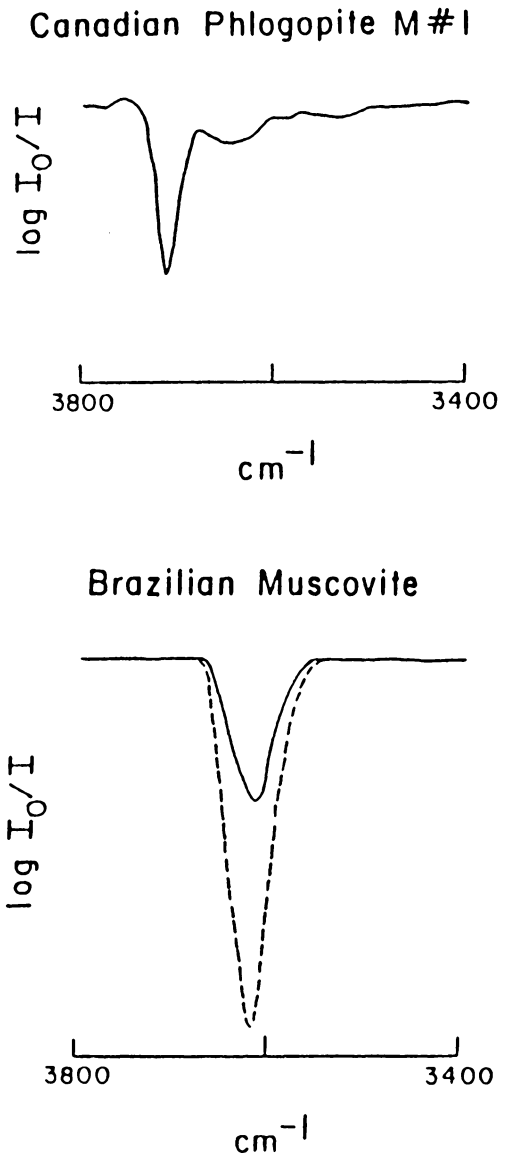

Figure 5.4 Hydroxyl stretching frequencies of muscovite and phlogopite
(modified after Vedder and Wilkins, 1969 and Vedder and McDonald, 1963)).

compared with the structural parameters of all of the selected structural analyses. Table 5.1 gives the Pearson correlation coefficient and significance level for the correlation between those parameters and the hydroxyl stretching frequencies. The correlation reflects that the M(1)O distance, the M(1)M(3) distance, the M(2)M(3) distance, the T(1)T(2) distance, and the OO distances in the M(1) cation site and the T(1)O(5)T(2), T(1)O(6)T(2), and T(1)O(7)T(1) angles will increase with decreasing hydroxyl stretching frequency, thus, decreasing thermal stability. But, in the T(2) tetrahedron both the average T(2)O distance and the OO distances will decrease with decreasing thermal stability. The cation distance changes and angle variations for the three cummingtonite-grunerite samples are consistent with the trend shown in Table 5.1 (See Tables 4.5, 4.6, and 4.7).

Systematic studies in the relationship between bonding and thermal stability of all hydrous minerals are needed to verify the significance of OH bond to the thermal stability of individual mineral systems.

Table 5.1 Pearson correlation coefficient and significance level between some structural parameters and hydroxyl stretching frequency

Parameter	R	P
T(2)O	0.65	0.027
OO(T2)	0.72	0.014
T(1)T(2)	-0.66	0.037
T(1)O(5)T(2)	-0.71	0.016
T(1)O(6)T(2)	-0.63	0.035
T(1)O(7)T(1)	-0.78	0.006
M(1)O	-0.77	0.007
M(1)M(3)	-0.72	0.020
M(2)M(3)	-0.87	0.002

REFERENCES

Addison, C.C., Addison, W.E., Neal, G.H. and Sharp, J.H. (1962a) Amphiboles Part I. The oxidation of crocidolite. Journal of Chemical Society, 278, 1468-1471.

_____, Neal, G.H. and Sharp, J.H. (1962b) Amphiboles Part II. The kinetics of the oxidation of crocidolite. Journal of Chemical Society, 278, 1472-1475.

Barnes, V.E. (1930) Changes in hornblende at about 800°. American Mineralogist, 15, 393-417.

Bancroft, G.M. and Burns, R.G. (1969) Mössbauer and absorption spectral study of alkali amphiboles. Mineralogical Society of America Special Paper 2, 137-148.

_____, Burns, R.G. and Maddock, A.G. (1967) Determination of the cation distribution in the cummingtonite-grunerite series by Mössbauer spectroscopy. American Mineralogist, 52, 1009-1026.

Bence, A.E. and Albee, A.L. (1968) Empirical correction factors of the electron microanalysis of silicates and oxides. Journal of Geology, 76, 382-403.

Bocchio, R., Ungaretti, L. and Rossi, G. (1978) Crystal chemistry study of eclogitic amphiboles from Alpe Arami, Lepontine Alps, southern Switzerland. Society of Italy Mineralogia Petrologia Rend, 34, 453-470.

Bonnichsen, B (1969) Metamorphic pyroxenesand amphiboles in the Biwabik iron formation, Dunka River Area, Minnesota. Mineralogical Society of America Special Paper 2, 217-239.

Boisen, M.B., Jr. and Gibbs, G.V. (1985) Mathematical Crystallography. Reviews in Mineralogy, 15.

Boyd, F.R. (1959) Hydrothermal investigation of amphiboles. in: Research in Geochemistry, Abelson, P.H., ed., 1, John Wiley & Sons Inc., New York. 377-396.

Brown, I.D. and Shannon, R.D. (1973) Empirical bond length-bond strength curves for oxides. Acta Crystallographica, A29, 282-299.

Burnham, C.W. (1966) Computation of absorption corrections, and the significance of end effect. American Mineralogist, 51, 159-167.

_____ (1986) LCLSQ - MARK VI, Least-squares refinement of crystallographic lattice parameters, IBM PC version, Harvard University, Cambridge, MA 02138

_____ , Holloway, J.R. and Davids, N.F. (1969) Thermodynamic properties of water to 1000°C and 10000 bars. Geological Society of America Special Paper 132, 96

Burns, R.G. and Strens, R.G.J. (1966) Infrared study of the hydroxyl bands in clinoamphiboles. Science, 153, 890-892.

_____ and Prentice, F.J. (1968) Distribution of iron cations in the crocidolite structure. American Mineralogist, 53, 770-776.

_____ and Law, A.D. (1970) Hydroxyl stretching frequencies in the infrared spectra of anthophyllites and gedrites. Nature, 226, 73-75.

_____ and Greaves, C.J. (1971) Correlation of infrared and Mössbauer site population measurements of actinolites. American Mineralogist, 56, 2010-2033.

Butler, P., Jr. (1969) Mineral compositions and equilibria in the metamorphosed iron formation of the Gagnon region, Quebec, Canada. Journal of Petrology, 10, 56-100.

Cameron, K.L. (1975) An experimental study of actinolite-cummingtonite phase relations with notes on the synthesis of Fe-rich anthophyllite. American Mineralogist, 60, 375-390.

Cameron, M. (1970) The crystal chemistry of tremolite and richterite. A study of selected anion and cation substitutions. Ph.D. thesis, Virginia Polytechnic Institute and State University, Blacksburg, Virginia.

_____ and Gibbs, G.V. (1971)Refinement of the crystal structure of two synthetic fluor-richterites. Carnegie Institute Washington Year Book 70, 150-153

_____ and Gibbs, G.V. (1973) The crystal structure and bonding of fluor-tremolite: A comparison with hydroxyl tremolite. American Mineralogist, 58, 879-888.

____and Papike, J.J. (1979) Amphibole crystal chemistry: A review. Fortschritte der Mineralogie, 57, 29-67.

_____, Sueno, S., Prewitt, C.T. and Papike, J.J. (1973a) High temperature crystal chemistry of K-fluor-richterite. American Geophysical Union Transactions, 54, 497-498 (abstract).

_____, _____, _____, and _____ (1973b) High temperature crystal chemistry of Na-fluor-richterite. American Geophysical Union Transaction, 54, 1230 (abstract).

Charles, R.W. (1974) The physical properties of the Mg-Fe richterites. American Mineralogist, 59, 518-528.

____ (1975) The phase equilibrium of richterite and ferrorichterite. American Mineralogist, 60, 367-374.

___ (1977) The phase equilibria of intermediate compositions on the pseudobinary $NaCaMg_5Si_8O_{22}(OH)_2$-$NaCaFe_5Si_8O_{22}(OH)_2$. American Journal of Science, 277, 594-625.

Chernosky, J.V. and Autio, L.K. (1979) The stability of anthophyllite in the presence of quartz. American Mineralogist, 64, 294-303.

Chyi, K., Gibbs, G.V. and Wones, D.R. (1982) Relationships between crystal structure, bonding and thermal stability of amphiboles. American Geophysical Union Transactions, 63, No. 18 (abstract).

Clark, M.W. and Freeman, A.G. (1967) Kinetics and mechanism of dehydroxylation of crocidolite. Transactions Farady Society, 63, 2051-2056.

Clementi, E. and Raimondi, D.L. (1963) Atomic screening constants from SCF functions. Journal of Chemical Physics, 38, 2686-2689.

Comeforo, J.E. and Kohn, J.A. (1954) Synthetic asbestos investigations. I: Study of synthetic fluor-tremolite. American Mineralogist, 39, 537-548.

Cromer, D.T. (1965) Anomalous dispersion correction computed from self-consistent field relativistic Dirac-Slater wave function. Acta Crystallographica, 18, 17-23.

Deer, W.A., Howie, R.A. and Zussman J. (1963) Rock-forming minerals, 2, Chain Silicates. Longmans, Green and Co., London.

DeVries, R.C. and Roy, R. (1958) Influence of ionic substitution on the stability of micas and chlorites. Economic Geology, 53, 958-965

Doyle, P.A. and Turner, P.S. (1968) Relativistic Hartree-Fock X-ray and electron scattering factors. Acta Crystallographica, A24, 390-397.

Ernst, W.G. (1960) Stability relations of magnesioriebeckite. Geochimica et Cosmochimica Acta, 19, 10-40.

____ (1962) Synthesis, stability relations,and occurrence of riebeckite and riebeckite-arfvedsonite solid solutions. Journal of Geology, 70, 689-736.

____ (1966) Synthesis and stability relations of ferrotremolite. American Journal of Science, 264, 37-65.

____ (1968) Amphiboles: Crystal Chemistry, Phase Relations and Occurrence. Springer-Verlag, New York, 128

___ and Wai, C.M. (1970) Infrared, X-ray and optical study of cation ordering and dehydrogenation in nature and heat treated sodic amphiboles. American Mineralogist, 55, 1226-1258.

Eugster, H.P. and Wones D.R. (1962) Stability relations of the ferruginous biotite, annite. Journal of Petrology, 3, 82-125.

Finger, L.W. (1969) The crystal structure and cation distribution of a grunerite. Mineralogical Society of America Special Paper 2, 95-100.

_____ (1970) Refinement of the crystal structure of an anthophyllite. Carnegie Institute Washington, Year Book 68, 283-288.

_____ and Prince, E. (1975) A system of FORTRAN IV computer programs for crystal structure computations. National Bureau of Standards Technical note 854.

Fischer, K.E. (1966) A further refinement of crystal structure of cummingtonite $(Mg,Fe)_7(Si_4O_{11})_2(OH)_2$. American Mineralogist, 51, 814-818.

Fonarev, VI. and Korolkov, G.Ja. (1980) The assemblage orthopyroxene + cummingtonite + quartz. The low temperature stability limit. Contributions to Mineralogy and Petrology, 73, 413-420.

_____, _____ and Dokina, T.N. (1976) Stability of the assamblage cummingtonite+quartz+magnetite association. Geokhimiya, 9, 1340-1353.

_____, _____ and _____ (1977) Experimental study of the assemblage cummingtonite+magnetite+quartz, $P = PH_2O = 1000$ kg/cm^2., NNO buffer. In Contribution to Physio-chemical Petrology, VI, Nauka, Moscow, 224-235.

_____, _____ and _____ (1979a) Stability fields in the assemblage cummingtonite-olivine-quartz from experimental evidence. Geochimica International, 15, 34-35.

_____, _____ and _____ (1979b) Experimental study in the assemblage orthopyroxene-olivine-quartz. In Problems of Physio-chemical Petrology, 1, Nauka, Moscow, 159-171.

Forbes, W.C. (1977) Stability relations of grunerite, $Fe_7Si_8O_{22}(OH)_2$. American Journal of Science, 277, 735-749.

Freeman, A.G. (1966) The dehydroxylation behaviour of amphiboles. Mineralogical Magazine, 35, 953-957.

Ghose, S. (1961) The crystal structure of a cummingtonite. Acta Crystallographica, 14, 622-627.

_____ and Hellner, E. (1959) The crystal structure of grunerite and observations on the Fe-Mg distribution. Journal of Geology, 67, 691-701.

Gibb, T.C. and Greenwood, N.N. (1965) Chemical application of the Mössbauer effect. 2. Oxidation state of iron in crocidolite and amosite. Transactions Farady Society , 61, 1317-1323.

Gibbs, G.V. (1966) American Geological Institute short course lecture notes on chain silicates, 1-23.

____(1986) Personal communication.

Gilbert, M.C. (1966) Synthesis and stability relationships of the hornblende ferroparagasite. American Journal of Science, 264, 698-742.

____ and Briggs, D.F. (1974) Comparison of the stabilities of OH and F-potassic richterites: A preliminary report. American Geophysical Union transactions, 55, 480-481.

_____, Helz, R.T., Popp, R.K. and Spear, F.S. (1982) Experimental studies of amphibole stability. Reviews in Mineralogy, 9b, 229-355.

Gole, M.J. and Klein, C. (1981) High-grade metamorphic Archean banded iron-formations, Western Australia: Assemblages with coexisting pyroxenes+fayalite. American Mineralogist, 66, 87-89.

Greenwood, H.J. (1963) The synthesis and stability of anthophyllite. Journal of Petrology, 4, 317-351.

Hadidiacos, C.G. (1969) Solid-state temperature controller. Journal of Geology, 77, 365-367.

Hamilton, W.C. (1959) On the isotropic temperature factor equivalent to a given anisotropic temperature factor. Acta Crystallographica, 12, 609-610

___(1965) Significance tests on the crystallographic R-factor. Acta Crystallographica, 18, 502-510.

Hafner, S.S. and Ghose, S. (1971) Iron and magnesium distribution in cummingtonites $(Mg, Fe)_7Si_8O_{22}(OH)_2$. Zeitschrift für Kristallographie, 133, 301-326.

Hawthorne, F.C. (1976) The crystal chemistry of amphiboles. V. The structure and chemistry of arfvedsonite. Canadian Mineralogist, 14, 346-356.

_____ (1983) The crystal chemistry of the amphiboles. Canadian Mineralogist, 21, 173-480.

_____ and Grundy, H.D. (1976) The crystal chemistry of the amphiboles. IV. X-ray and neutron refinement of crystal structure of tremolite. Canadian Mineralogist, 41, 43-50.

Hazen, R.M. and Prewitt, C.T. (1977) Effects of temperature and pressure on interatomic distances in oxygen-based minerals. American Mineralogist, 62, 309-315.

Hewitt, D.A. (1978) A redetermination of the fayalite-magnetite-quartz equilibrium between 650° and 850°. American Journal of Science, 278, 715-724.

Hodgson, A.A. (1965) The thermal decomposition of miscellaneous crocidolites. Mineralogical Magazine, 35, 291-305.

_____, Freeman, A.G. and Taylor, H.F.W. (1965) The thermal decomposition of crocidolite from Koegas, South Africa. Mineralogical Magzine, 35, 5-30.

Holdaway, M.J. (1972) Thermal stability of Al-Fe epidote as a function of fO_2 and Fe content. Contributions to Mineralogy and Petrology, 37, 307-340.

Immega, I.P. and Klein, C. (1976) Mineralogy and petrology of some metamorphic Precambrian iron-formations in southwestern Montana. American Mineralogist, 61, 1117-1144.

Kiefer, C. (1949) Deshydration thermique des mineraux phylliteux. C. R. Academy of Science Paris, 229, 1021-1022.

Klein, C., Tr. (1964) Cummingtonite - grunerite series: a chemical, optical and x-ray study. American Mineralogist, 49, 963-982.

_____ (1978) Regional metamorphism of Proterozoic iron-formations, Labrador Trough, Canada. American Mineralogist, 63, 898-912.

_____and Waldbaum, D.R. (1967) X-ray crystallographic properties of the cummingtonite-grunerite series. Journal of Geology, 75, 379-392.

Kunitz, W. (1930) Die Isomorphieverhaeltnisse in der Hornblende-gruppe. Neues Jahrbuch für Mineralogie Abhandlungen, 60, 171-250.

Langer, K. and Raith, M. (1974) Infrared spectra of Al-Fe(III)-epidotes and zoisites, $Ca_2(Al_{1-p}Fe^{+3}_p)Al_2O(OH)[Si_2O_7][SiO_4]$. American Mineralogist, 59, 1249-1258

Lazarev, A.N. (1972) Vibrational Spectra and the Structure of Silicates. Plenum Press, New York.

Leake B.E. (1978) Nomenclature of amphiboles. Canadian Mineralogist, 16, 501-520.

Littler, J.G.F. and Williams, R.J.P. (1965) Electricial and optical properties of crocidolite and some other compounds. Journal of Chemical Society, 1965, 6368-6371.

Litvin, A.L. (1973) Calcic Amphiboles (Structure, Cation Distribution, Unit Cell Dimensions). Naukova Dumka, Kiev (in Russian).

_____, Michnik, T.L., Petrunina, A.A., Pol'shin, E.V., Efimov, A.F. and Kovalenko, V.I. (1976) Structure and some characteristics of the crystal chemistry of amphiboles. Konst. Svoistva Mineral., 10, 3-9.

Makino, K and Tomita K., (1986) Cation order-disorder in octahedral sites (M1, M2 and M3) of hornblendes. Abstract, International Mineralogical Association, 1986, 163-164.

Maresch, W.V. and Czank M., (1983) Phase characterization of syntheric amphiboles on the join $(Mg_{7-x}, Mn^{+2}{}_x)Si_8O_{22}(OH)_2$. American Mineralogist, 68, 744-753

McDonald, W.S. and Cruickshank, D.W.J. (1967) A re-investigation of the structure sodium metasilicate, Na_2SiO_3. Acta Crystallographica, 22, 37-43.

Mitchell, J.T., Bloss, F.D. and Gibbs, G.V. (1971) Examination of the actinolite structure and four other C2/m amphiboles in terms of double bonding. Zeitschrift für Kristallographie, 133, 449-497.

Morey, G.B., Papike, J.J., Smith, R.W. and Weiblen, P.W. (1972) Observations on the contact metamorphism of the Biwabik Iron Formation, East Messabic District, Minnesota. Geological Society of America Memoir 135, 225-264.

Mottana, A. and Griffin, W.L. (1986) Crystal chemistry of two coexisting K-richterites from St. Marcel (Val d'Aosta, Italy). American Mineralogist, 71, 1426-1433.

Ohashi, Y. and Burnham, C.W. (1972) Electrostatic and repulsive energies of the M1 and M2 cation sites in pyroxenes. Journal of Geophysical Research, 77, No.29, 1-20.

_____(1976) ELEN2: A FORTRAN program for electrostatic energy calculation.

Papike, J.J., Ross, M. and Clark, J.R. (1969) Crystal-chemical characterization of clinoamphiboles based on five new structure refinements. Mineralogical Society of America Special Paper 2, 117-136.

Patterson, J.H. and O'Connor, D.J. (1966) Chemical studies of amphibole asbestos. I. Structural changes of heat-treated crocidolite, amosite, and tremolite from infrared absorption studies. Australian Journal of Chemistry, 19, 1155-1164.

Phillips, M.W., Popp, R.K. and Pinkerton, A.A. (1986) Structural investigation of oxidation-dehydroxylation in hornblende. American Geophysical Union Transactions, 67, 1270 (abstract).

Popp, P.K., Gilbert, M.C. and Craig, J.R. (1976) Synthetic and X-ray properties of Fe-Mg orthoamphiboles. American Mineralogist, 61, 1267-1279.

Prewitt, C.T., Papike, J.J. and Ross, M. (1970) Cummingtonite : A reversible, nonquenchable transition from $P2_1/m$ to C2/m symmetry, Earth and Planetary Science Letters, 8, 448-450.

Robinson, K., Gibbs, G.V., Ribbe, P.H., and Hall, M.R. (1973) Cation distribution in three hornblendes. American Journal of Science, Cooper Volume 273-A, 522-535.

Ross, M., Papike, J.J. and Weiblen, P.W. (1968) Exsolution in clinoamphiboles. Science , 159, 1099-1102

_____ , _____ and Shaw, K.W. (1969) Exsolution textures in amphiboles as indicators of subsolidus thermal histories. Mineralogical Society of America Special Paper 2, 275-299.

Rowbothan, G. and Farmer, V.C. (1973) The effect of "A" site occupancy on the hydroxyl stretching frequency in clinoamphiboles. Contributions to Mineralogy and Petrology, 38, 147-149.

Semet, U.P. (1973) A crystal-chemical study of synthetic magnesiohastingsite. American Mineralogist, 58, 480-494.

_____ and Ernst, W.G. (1981) Experimental stability relations of hornblende magnesiohastingsite. Geological Society of America Bulletin, 92, 71-74.

Strens, R.G.J. (1963) Some relationships between members of the epidote group, Nature, 198, 80-81.

_____ (1966) Infrared study of cation ordering and clustering in some (Fe,Mg) amphibole solid solutions. Chemical Communications, 15, 519-520.

_____ (1974) The common chain, ribbon, and ring silicates. in The Infrared Spectra of Minerals. Mineralogical Society, London, 305-330.

Sueno, S., Papike, J.J., Prewitt, C.T. and Brown, G.E. (1972) Crystal structure of high cummingtonite. Journal of Geophysical Research, 77, 5767-5777.

_____, Cameron, M., Papike, J.J. and Prewitt, C.T. (1973) The high temperature crystal chemistry of tremolite. American Mineralogist, 58, 649-664.

Thomas, W.M. (1977) Preliminary stability relations of the hornblende hastingsite and the effect of Fe^{3+} for aluminum replacement in amphiboles. (abs.) American Geophysical Union Transactions, 58, 1244.

_____ (1982) Stability relations of the amphibole hastingsite. American Journal of Science, 282, 136-164.

Troll, G. and Gilbert, M.C. (1972) Fluorine-hydroxyl substitution in tremolite. American Mineralogist, 57, 1380-1403.

Tuttle, O.F. (1949) Two pressure vessels for silicate-water studies. Geological Society of America Bulletin, 60, 1727-1729.

Vaniman, D.T., Papike, J.J. and Labotka, T. (1980) Contact-metamorphic effects of the Stillwater Complex, Montana: the concordant iron formation. American Mineralogist, 65, 1087-1102.

Vedder, W. (1964) Correlations between infrared spctrum and chemical composition of mica, American Mineralogist, 49, 736-768.

_____ and McDonald, R.S. (1963) Vibrations of the OH ions in muscovite. Journal of Chemical Physics, 38, 1538-1590.

_____ and Wilkins, R.W.T. (1969) Dehydroxylation and rehydroxylation, oxidation and reduction of micas. American Mineralogist, 54, 482-509.

Viswanathan, K. and Ghose, S. (1965) The effect of Mg^{2+}-Fe^{2+} substitution on the cell dimensions of cummingtonites. American Mineralogist, 50, 1106-1112.

Whittaker, E.J.W. (1949) The structure of Bolivian crocidolite. Acta Crystallographica, 13, 312-317.

Wilkins, R.W.T. (1970) Iron-madnesium distribution in the tremolite-actinolite series. American Mineralogist, 55, 1993-1998.

Wones, D.R. (1981) Mafic silicates as indicators of variables in granitic magmas. Japan Mining Geology, 31(4), 191-212.

Yoder, H.S. and Eugster, H.P. (1954) Phlogopite synthesis and stability range. Geochimica et Cosmochimica Acta, 6, 157-185.

_____ and _____ (1955) Synthetic and natural muscovite. Geochimica et Cosmochimica Acta, 8, 225-280.

Appendix A

Infrared spectra and chemical analyses of samples used in this study.

Table A.1 Chemistry of Cummingtonite-Grunerite Samples

Sample	140621	96768	143350	118125	143288	134018
SiO_2	57.76	57.68	55.73	55.09	55.75	52.23
TiO_2	0.01	0.02	0.07	0.01	0.02	0.03
Al_2O_3	0.12	0.19	0.34	0.24	0.22	0.38
FeO	0.21	10.48	16.86	20.09	5.06	28.99
MgO	26.51	27.90	23.25	20.44	18.73	13.96
MnO	9.13	0.37	0.34	0.61	17.58	1.21
CaO	2.84	0.48	0.48	0.87	0.94	0.51
BaO	0.00	0.00	0.01	0.00	0.01	0.03
Na_2O	0.25	0.10	0.09	0.06	0.10	0.04
K_2O	0.00	0.00	0.02	0.00	0.00	0.01
H_2O(N.D.)	0.00	0.00	0.00	0.00	0.00	0.00
F^-	0.27	0.63	0.01	0.03	0.00	0.06
Cl^-	0.00	0.00	0.00	0.00	0.01	0.00
Total	97.10	97.85	97.20	97.44	98.42	97.45
Total Anions	24	24	24	24	24	24
Si	7.98	7.94	7.92	7.95	8.01	7.91
Al	0.02	0.03	0.06	0.04	0.04	0.07
Ti	0.00	0.00	0.01	0.00	0.00	0.00
Fe^{+2}	0.02	1.21	2.00	2.42	0.61	3.67
Mg	5.46	5.73	4.93	4.40	4.01	3.15
Mn	1.07	0.04	0.04	0.07	2.14	0.16
Ca	0.42	0.07	0.07	0.13	0.14	0.08
Ba	0.00	0.00	0.00	0.00	0.00	0.00
Na	0.07	0.03	0.02	0.02	0.03	0.01
K	0.00	0.00	0.00	0.00	0.00	0.00
OH^-	1.88	1.73	2.00	1.99	2.00	1.97
F^-	0.12	0.27	0.00	0.01	0.00	0.03
Cl^-	0.00	0.00	0.00	0.00	0.00	0.00
$Si+Al^{IV}$	8.00	7.97	7.98	7.99	8.01	7.98
$Al^{VI}+FM+Zn+Ti$	6.55	6.98	6.98	6.90	6.80	6.98
Ca+Ba+Na+K	0.49	0.10	0.10	0.15	0.17	0.10
$OH^-+F^-+Cl^-$	2.00	2.00	2.00	2.00	2.00	2.00
Fe/Fe+Mg	0.00	0.17	0.29	0.36	0.13	0.54
Fe+Mn/Fe+Mn+Mg	0.17	0.18	0.29	0.36	0.41	0.55

Table A.1 continued:

Sample	K.No.10A	133791	R16782	124274	11749	K.No.9A
SiO_2	52.28	50.88	51.05	51.60	50.75	49.33
TiO_2	0.00	0.11	0.03	0.04	0.03	0.02
Al_2O_3	0.07	1.41	0.00	0.05	0.31	0.39
FeO	31.90	32.31	35.98	26.06	37.88	40.94
MgO	12.35	11.64	8.73	8.59	6.46	6.65
MnO	0.57	0.32	0.96	10.75	0.94	0.54
CaO	0.79	1.04	0.97	0.97	0.20	0.18
BaO	0.00	0.03	0.05	0.04	0.03	0.00
Na_2O	0.12	0.27	0.02	0.03	0.06	0.12
K_2O	0.08	0.04	0.02	0.01	0.02	0.20
H_2O(N.D.)	0.00	0.00	0.00	0.00	0.00	0.00
F^-	0.00	0.07	0.03	0.38	0.12	0.00
Cl^-	0.00	0.09	0.06	0.03	0.00	0.00
Total	98.16	98.21	97.90	98.55	96.80	98.37
Total Anions	24	24	24	24	24	24
Si	7.95	7.78	7.98	8.01	8.08	7.86
Al	0.01	0.25	0.00	0.01	0.06	0.07
Ti	0.00	0.01	0.00	0.00	0.00	0.00
Fe^{+2}	4.06	4.13	4.70	3.38	5.04	5.45
Mg	2.80	2.65	2.03	1.99	1.53	1.58
Mn	0.07	0.04	0.13	1.41	0.13	0.07
Ca	0.13	0.17	0.16	0.16	0.03	0.03
Ba	0.00	0.00	0.00	0.00	0.00	0.00
Na	0.04	0.08	0.01	0.01	0.02	0.04
K	0.02	0.01	0.00	0.00	0.00	0.04
OH^-	2.00	1.94	1.97	1.81	1.94	2.00
F^-	0.00	0.03	0.01	0.19	0.06	0.00
Cl^-	0.00	0.02	0.02	0.01	0.00	0.00
$Si+Al^{IV}$	7.96	8.00	7.98	8.01	8.08	7.93
Al^{VI}+FM+Zn+Ti	6.93	6.87	6.87	6.80	6.76	7.11
Ca+Ba+Na+K	0.18	0.26	0.18	0.17	0.06	0.11
$OH^-+F^-+Cl^-$	2.00	2.00	2.00	2.00	2.00	2.00
Fe/Fe+Mg	0.59	0.61	0.70	0.63	0.77	0.78
Fe+Mn/Fe+Mn+Mg	0.60	0.61	0.70	0.71	0.77	0.78

Table A.1 continued:

Sample	R2956	97557	K.No.1	R3190	153602	R7702
SiO_2	50.02	50.31	49.01	48.96	48.46	48.44
TiO_2	0.03	0.04	0.05	0.04	0.05	0.04
Al_2O_3	0.58	0.20	0.00	0.27	0.38	0.19
FeO	38.27	38.53	44.99	46.81	46.25	6.49
MgO	6.24	5.76	3.17	1.94	1.04	0.01
MnO	1.22	1.88	0.37	0.15	0.23	1.70
CaO	0.30	0.40	0.31	0.13	1.04	0.05
BaO	0.01	0.04	0.00	0.03	0.14	0.14
Na_2O	0.11	0.05	0.04	0.04	0.05	0.14
K_2O	0.08	0.02	0.00	0.02	0.04	0.03
H_2O(N.D.)	0.00	0.00	0.00	0.00	0.00	0.00
F^-	0.02	0.04	1.00	0.28	0.03	0.13
Cl^-	0.00	0.02	0.00	0.00	0.04	0.05
Total	96.88	97.29	98.94	98.67	97.75	97.33
Total Anions	24	24	24	24	24	24
Si	7.99	8.04	7.99	8.00	8.00	8.08
Al	0.11	0.04	0.00	0.05	0.07	0.04
Ti	0.00	0.00	0.01	0.00	0.01	0.01
Fe^{+2}	5.11	5.15	6.13	6.39	6.38	6.49
Mg	1.49	1.37	0.77	0.47	0.26	0.00
Mn	0.17	0.25	0.05	0.02	0.03	0.24
Ca	0.05	0.07	0.05	0.02	0.18	0.01
Ba	0.00	0.00	0.00	0.00	0.01	0.00
Na	0.03	0.02	0.01	0.01	0.02	0.05
K	0.02	0.00	0.00	0.00	0.01	0.01
OH^-	1.99	1.97	1.48	1.86	1.97	1.92
F^-	0.01	0.02	0.52	0.14	0.02	0.07
Cl^-	0.00	0.01	0.00	0.00	0.01	0.01
$Si+Al^{IV}$	8.00	8.04	7.99	8.00	8.00	8.08
$Al^{VI}+FM+Zn+Ti$	6.87	6.82	6.96	6.94	6.75	6.77
Ca+Ba+Na+K	0.10	0.09	0.07	0.04	0.22	0.06
$OH^-+F^-+Cl^-$	2.00	2.00	2.00	2.00	2.00	2.00
Fe/Fe+Mg	0.77	0.79	0.89	0.93	0.96	1.00
Fe+Mn/Fe+Mn+Mg	0.78	0.80	0.89	0.93	0.96	1.00

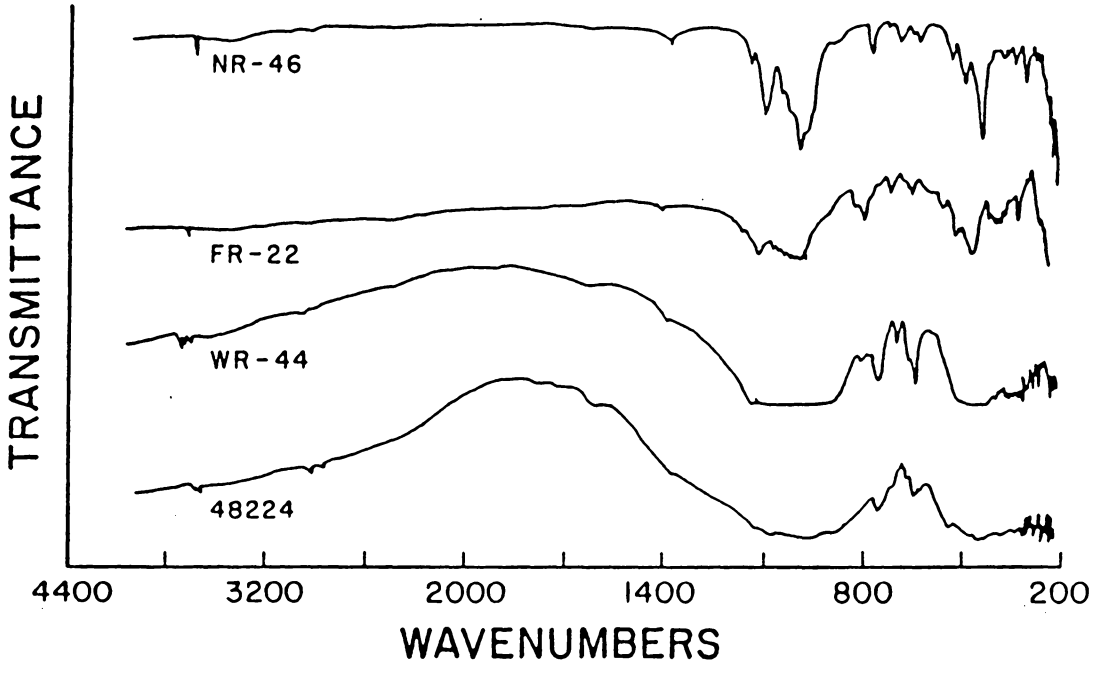

Figure A.1 Infrared spectra of riebeckite-arfvedsonite.

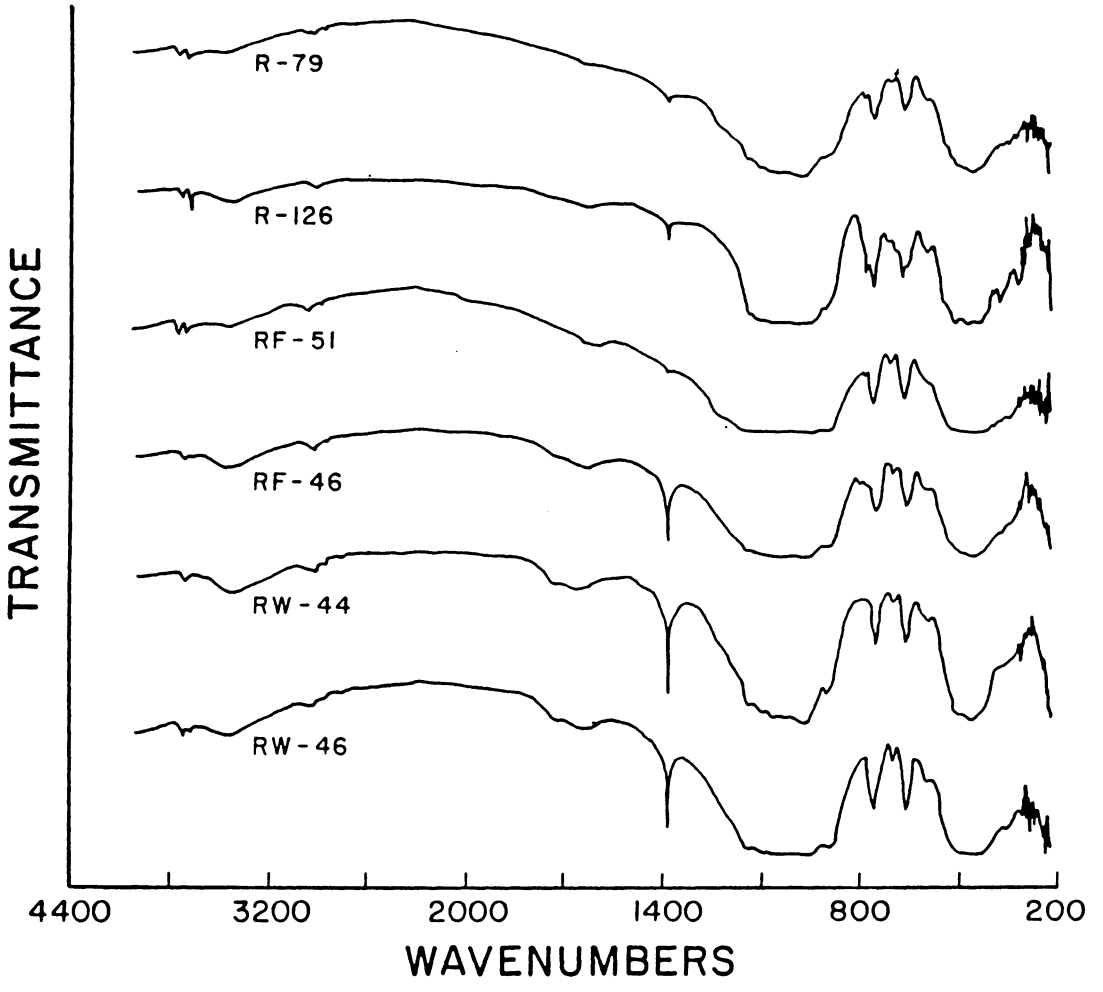

Figure A.2 Infrared spectra of magnesioriebeckite.

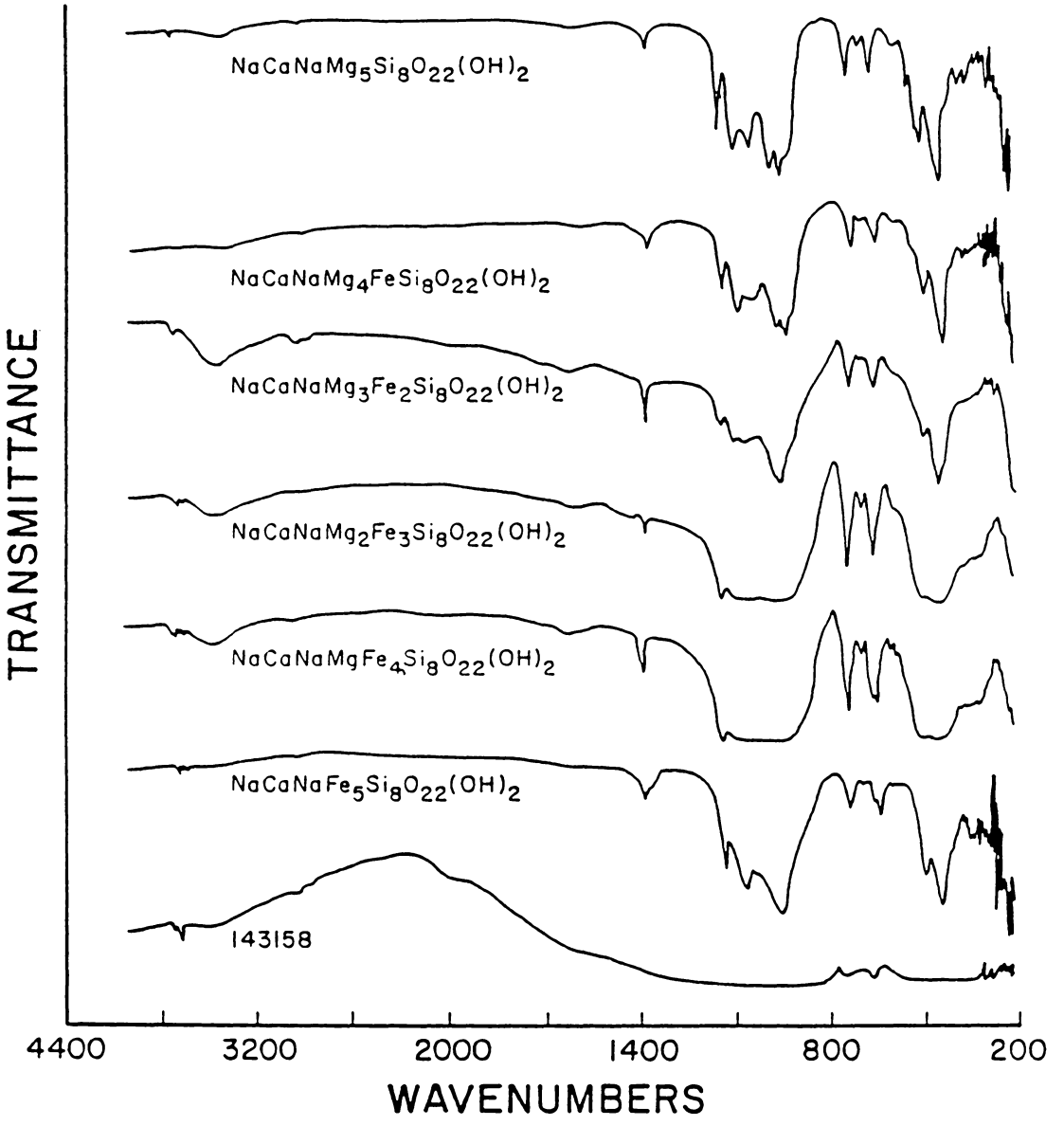

Figure A.3 Infrared spectra of richterite-ferrorichterite.

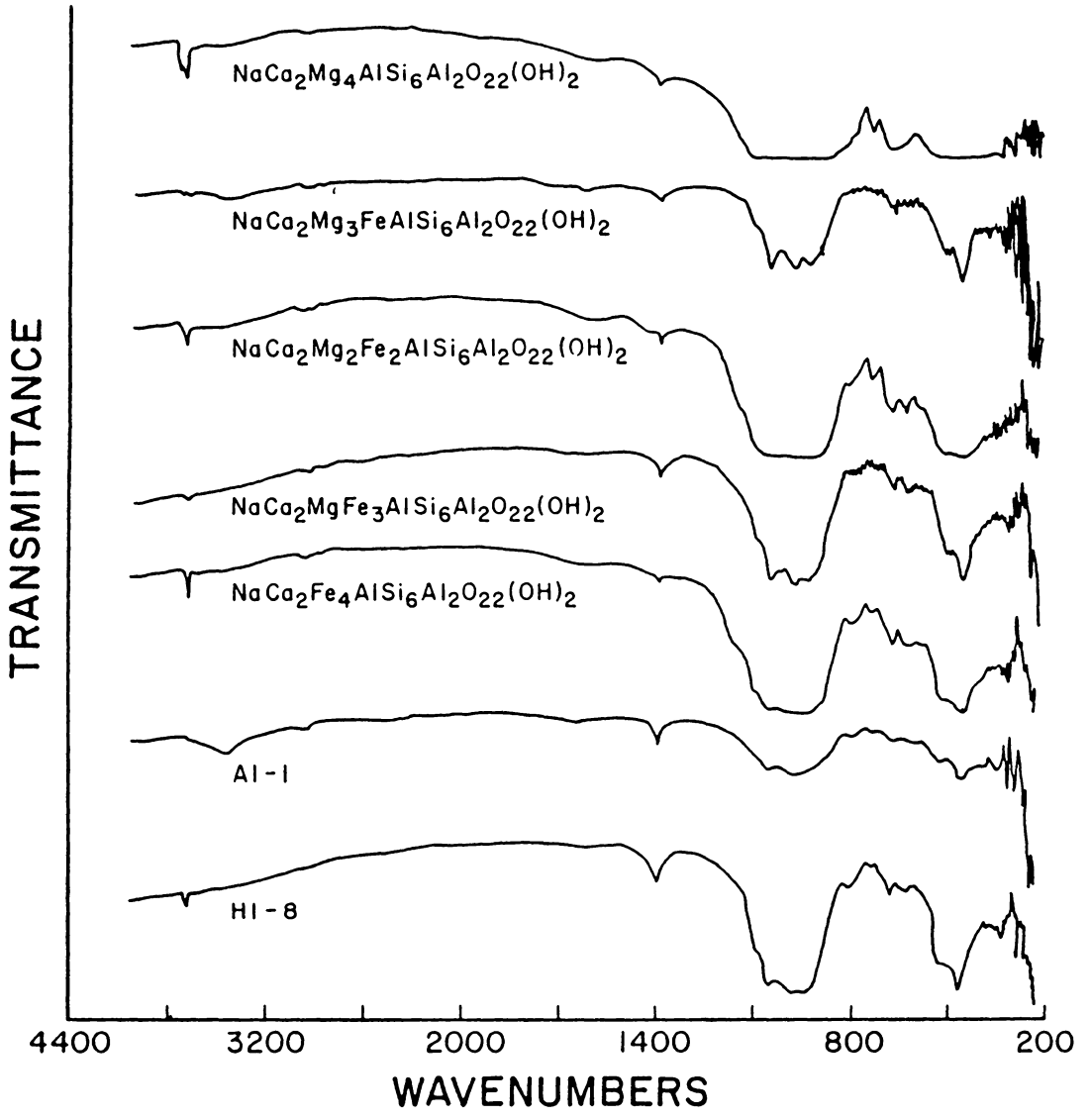

Figure A.4 Infrared spectra of pargasite-ferropargasite series.

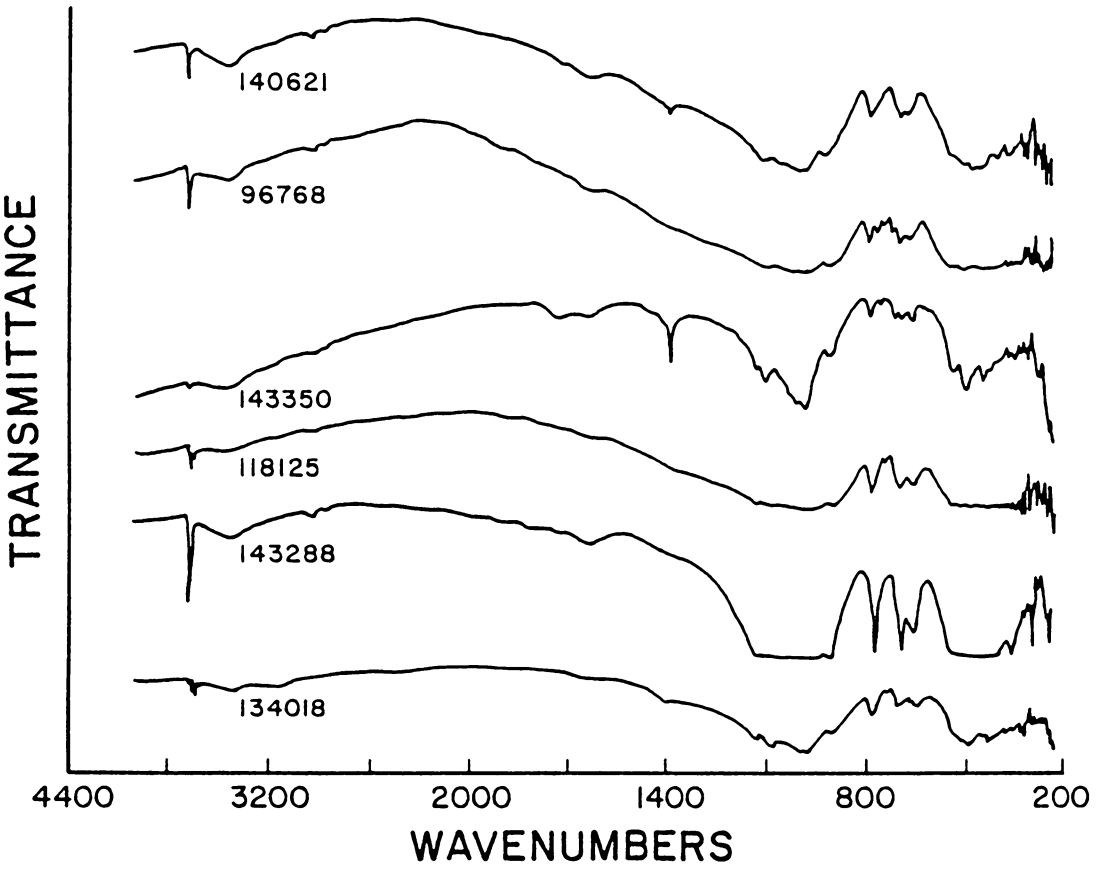

Figure A.5 Infrared spectra of cummingtonite-grunerite series.

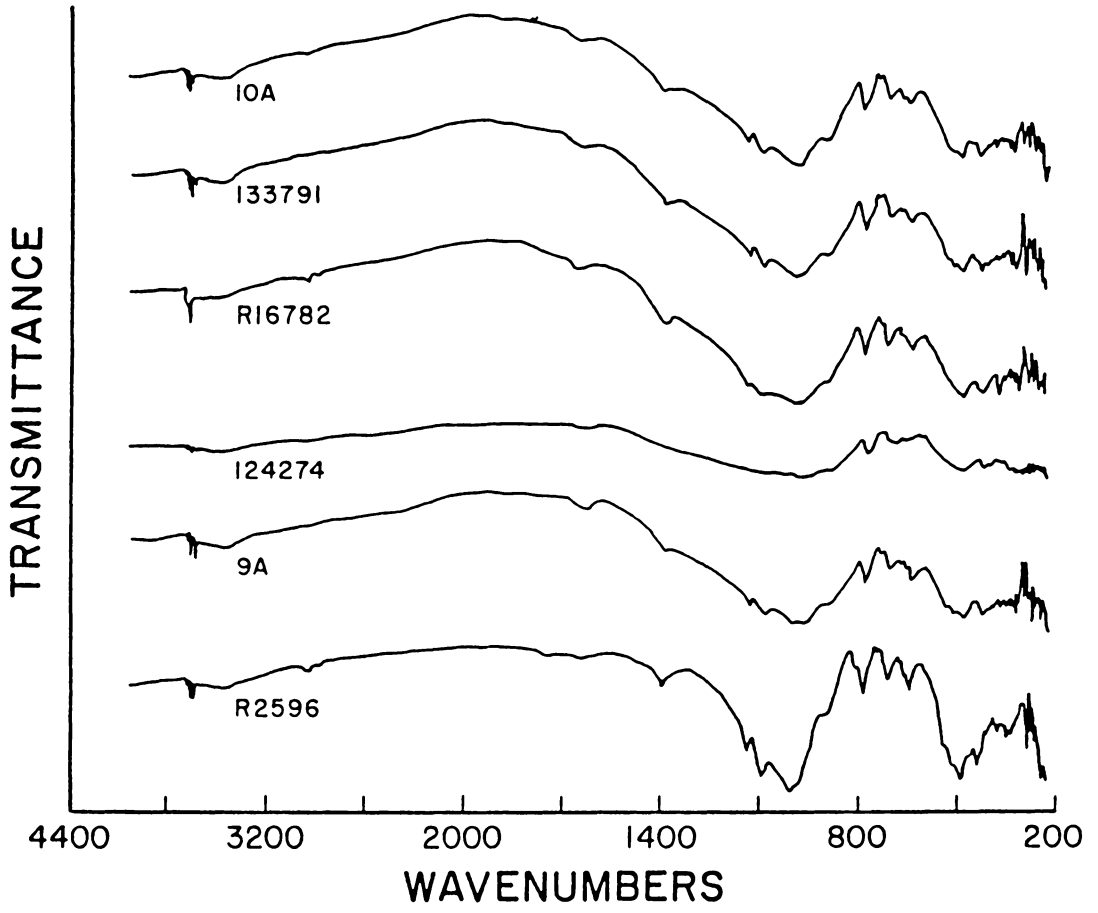

Figure A.5 Infrared spectra of cummingtonite-grunerite series. (continued)

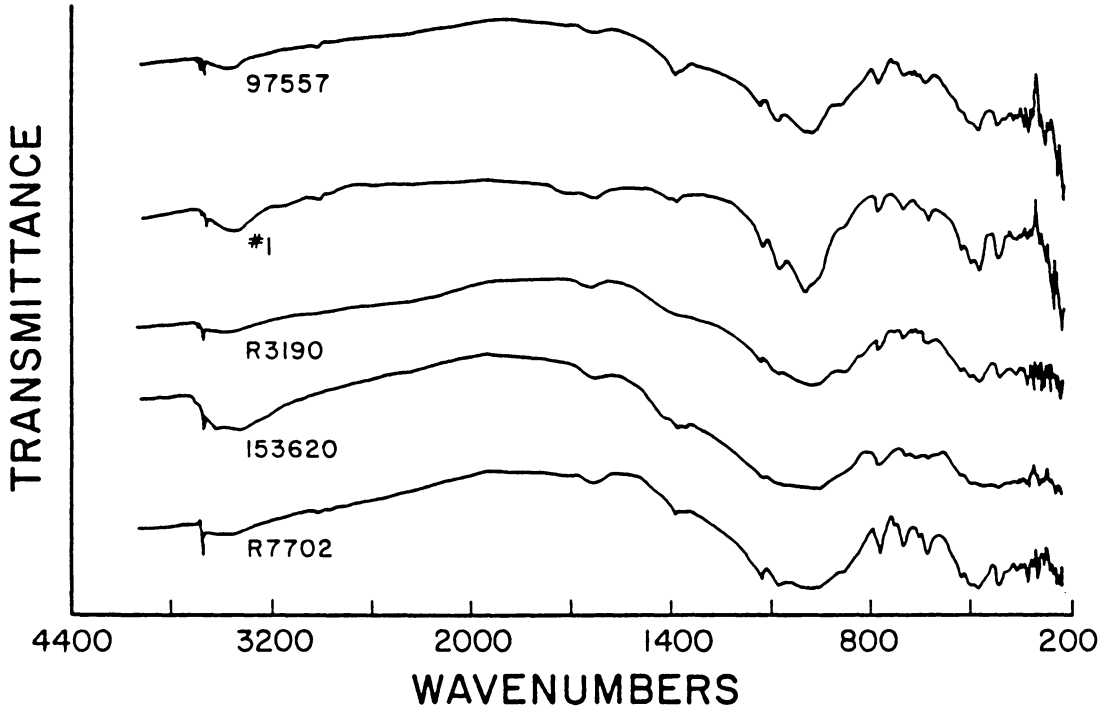

Figure A.5 Infrared spectra of cummingtonite-grunerite series. (continued)

The two page vita has been removed from the scanned document. Page 1 of 2

The two page vita has been removed from the scanned document. Page 2 of 2